Drosophila nicotinic acetylcholine receptor subunits and their native interactions with insecticidal peptide toxins

Dagmara Korona (1) *, Benedict Dirnberger (1, 2) *, Carlo N. G. Giachello (4)*, Rayner M. L. Queiroz (2), David-Paul Minde (2), Michael J. Deery (2), Glynnis Johnson (1), Karin H. Müller (3), Lucy C. Firth (4), Fergus G. Earley (4), Steven Russell (1) ** and Kathryn S. Lilley (5) **

(1) Department of Genetics, University of Cambridge, Downing Street, Cambridge, CB2 3EH, United Kingdom

(2) Cambridge Centre for Proteomics, Department of Biochemistry, Gleeson Building, University of Cambridge, Tennis Court Road, Cambridge, CB2 1GA, United Kingdom

(3) Cambridge Advanced Imaging Centre, Department of Physiology, Development and Neuroscience/Anatomy Building, University of Cambridge, Downing Street, CB2 3DY, United Kingdom

(4) Syngenta, Jealott's Hill International Research Centre, Bracknell, RG42 6EY, United Kingdom

(5) Cambridge Centre for Proteomics, Department of Biochemistry, Gleeson Building, University of Cambridge, Tennis Court Road, Cambridge, CB2 1GA, United Kingdom. k.s.lilley@bioc.cam.ac.uk

*These authors contributed equally: Dagmara Korona, Benedict Dirnberger, Carlo N. G. Giachello

**Correspondence should be addressed to Kathryn S. Lilley k.s.lilley@bioc.cam.ac.uk and Steven Russell sr120@cam.ac.uk

Abstract

Drosophila nicotinic acetylcholine receptors (nAChRs) are ligand-gated ion channels that present a target for insecticides. However, a better understanding of receptor subunit composition is needed for effective design of insecticides. Peptide neurotoxins are known to block nAChRs by binding to its target subunits. To facilitate the analysis of nAChRs we used a CRISPR/Cas9 strategy to generate null alleles for all ten *nAChR* subunit genes. We studied interactions of nAChR subunits with peptide neurotoxins by larval injections and styrene maleic acid lipid particles (SMALPs) pull-down assays. For the null alleles we determined the effects of α-Bungarotoxin (α-Btx) and ω-Hexatoxin-Hv1a (Hv1a) administration, identifying potential receptor subunits implicated in the binding of these toxins. We employed pull-down assays to confirm α-Btx interactions with the Dα5, Dα6, Dα7 subunits. Finally, we report the localization of fluorescent tagged endogenous Dα6 during nervous system development. Taken together this study elucidates native *Drosophila* nAChR subunit interactions with insecticidal peptide toxins.

Introduction

Global climate change and other factors are placing increasing demands on available agricultural land to deliver efficient, reliable and sustainable food production. Insecticides are important tools in securing yields of all major crops but need to be continually replaced to overcome resistance in target species and reduce environmental impacts. In addition, new insecticides must have low toxicity to non-target species, particularly the major pollinators essential for agriculture. A large class of insecticide targets are neurotransmitter receptors such as the nicotinic acetylcholine receptors (nAChRs) located in synaptic plasma membranes[1]. These pentameric cys-loop ligand-gated ion channels consist of either only α-subunits or α- and β-subunits, with ligand binding sites located between two α-subunits or between α- and β-subunits. Most insect genomes, including that of the highly tractable *Drosophila melanogaster* model, harbour ten highly conserved subunit genes that assemble in various combinations to form the active receptors.

An essential pre-requisite for effective design of new insecticides targeting these receptors is understanding the subunit composition of nAChRs and their distinctive binding properties. For a variety of reasons, including low expression in endogenous tissues or difficulties in expressing insect receptors in heterologous systems, the characterisation of functional insect receptors has been challenging[2,3,4]. Even in the tractable *D. melanogaster* insect model, there has until recently been no systematic isolation of mutations in *nAChR* subunit genes. Perry and colleagues described the generation of a new set of null mutations in nine out of the ten *D. melanogaster* subunit genes, however, these were generated in different genetic backgrounds necessitating additional work to assay background sensitive phenotypes such as neural or behavioural defects[2].

Several classes of insecticide, the most effective being neonicotinoid and spinosad molecules, have been shown to bind insect nAChRs highly selectively to block their functions[5,6]. Recently, the binding affinity and the positive allosteric effect of ω-Hexatoxin-Hv1a (Hv1a) peptide on nAChRs have been demonstrated[5]. These peptides isolated from spider venoms are well known for their insecticidal effects. Alongside these, other peptide toxins, such snake venom constituent, α-Bungarotoxin (α-Btx), have been widely used to probe nAChR functions but whether α-Btx contains a selective insecticidal property is currently unknown. Alpha-Btx is a 74 amino acid peptide that binds irreversibly to nAChR α-subunits in different species, including *D. melanogaster*, although the exact subunit composition of target receptors is not

fully understood[7,8,9]. Landsdell and co-workers have shown binding of α-Btx to *D. melanogaster* Dα5, Dα6, and Dα7 subunits in a heterologous S2 cell expression system[10,11] and the amino acid sequence of these subunits show strong similarity in their ligand-binding domains (LBD).

The lipid bilayer surrounding nAChRs is known to be essential for structural integrity, stability and ligand binding[12]. However, this lipid requirement can make analysis of membrane protein complexes challenging. The development of methods for extracting membrane proteins from lipid bilayers using detergents and introducing them into artificial lipid nanodiscs has facilitated a much better characterisation of receptor-ligand interactions[13]. However, the detergents generally used to solubilize membrane proteins lead to destabilisation, aggregation and misfolding and are therefore not compatible with this type of analysis[14]. Styrene maleic acid lipid particles (SMALPs) allow detergent-free extraction of membrane proteins in their local lipid environment and represent a promising technique for investigating receptor-ligand interactions under native conditions[15]. This is particularly important since loss of lipids surrounding membrane proteins can lead to changes in measured binding affinities[16,17]. The combination of detergent free SMALPs extraction coupled with mass spectrometry analysis provides a potential route for characterising native membrane receptor complexes[18,19].

Here we report the results from a combined genetic and biochemical analysis of *D. melanogaster* nAChRs *in vivo*. Using CRISPR/Cas9 genome engineering we generated new null mutations for all ten receptor subunit genes in a uniform genetic background as well as introducing fluorescent protein into the *nAChRα6* locus. We show that the null mutants in all seven α-subunit genes and two of the three β-subunit genes are viable and fertile, although we find mild morphological defects and some neurological impairment. Mutation of the remaining subunit gene, *nAChRβ1*, is recessive lethal. All nine of the viable null mutants were used to demonstrate a novel selective insecticidal effect of α-Btx on the *nAChRα5, nAChRα6* and *nAChRα7* subunits. We also applied the insecticidal Hv1a peptide to the viable null mutants, showing resistance in two subunit gene mutants: *nAChRα4* and *nAChRβ2*. In our biochemical studies we analysed receptor-ligand interactions in native conditions using SMALPs to verify the *in vivo* receptor subunit composition of the α-Btx binding target in adult neural tissue from wild-type and receptor subunit mutants. Our analysis revealed binding of α-Btx to receptors containing Dα5, Dα6 and Dα7 subunits with the analysis of mutants in these subunits genes indicating heterogeneity in α-Btx binding nAChRs.

Furthermore, we have identified specific glycosylation sites in Dα5 and Dα7 subunits which are known from other studies to play a critical role in α-Btx binding affinity[20,8]. Localization studies with the Dα6 subunit tagged at the endogenous locus with a fluorescent reporter shows expression at different developmental stages in specific neuronal cells, including the Kenyon cells of the mushroom bodies, a known site of α-Btx-binding.

Results

Mutating *D. melanogaster* nicotinic acetylcholine receptor subunit genes

To investigate the role of individual nAChR subunits we used CRISPR/Cas9 to generate deletion mutations in each of the seven α-subunit and three β-subunit genes. All of the mutations were generated in virtually identical genetic backgrounds using nanos-Cas9 insertions on the second or third chromosome. In brief, for each gene we targeted exons shared between all predicted isoforms, close to the N-terminus of the protein. In order to disrupt each coding sequence and facilitate screening we introduced a visible fluorescent marker, DsRED under control of the eye-specific 3xP3 promoter at the targeted locus. Positive lines were confirmed by PCR and sequencing, and subsequently the DsRED marker was excised from the genome by Cre-Lox recombination. For nine out of ten subunit genes we established homozygous viable and fertile stocks, the exception was the *nAChRβ1* gene which proved to be recessive lethal. Although all the other lines are viable, we noticed that several of the mutants, particularly *nAChRα1, nAChRα2, nAChRα6* and *nAChRβ2*, exhibited a curled abdomen phenotype that is most prominent in males (25, 20, 15 and 15 % males respectively) (Fig. 1A). It is possible that this phenotype is a result of defects in neural control of abdominal muscles and it is interesting to note that a previous analysis of an *nAChRα1* allele reports reduced male courtship and mating[21].

Since nAChRs are mostly found in the nervous system, we carried out basic climbing assays on the null alleles to assess potential locomotor defects (Fig. 1B). We saw little or no impact on the locomotor activity of ten day old flies with *nAChRα4, nAChRα5, nAChRα7, nAChRβ2* or *nAChRβ3*, homozygous mutants, however, deletion strains of *nAChRα1*, *nAChRα2* and *nAChRα6* showed 50-60 % reductions in climbing ability compared to wild-type. In contrast, the *nAChRα3* null mutant and heterozygotes for *nAChRβ1* exhibited a severe reduction in locomotor activity to less than 40 % of wild-type (22% and 34% respectively).

Taken together, we report the generation and validation of null mutations in all ten *D. melanogaster nAChR* subunit genes. Phenotype of all *nAChR* α-subunits, *nAChRβ2* and *nAChRβ3* deletion strains showed mild morphological defects. Deleting the *nAChRβ1* gene results in recessive lethal *D. melanogaster* progeny. Locomotor activity assayed by climbing tests showed distinctly reduced mobility in *nAChR* null alleles.

Distinct nAChR subunits mediate interactions with ω-Hexatoxin-Hv1a and α-Bungarotoxin

In order to investigate the selective contribution of each *nAChR* subunits to toxin binding *in vivo*, we injected the homozygous *nAChR* null mutants with either ω-Hexatoxin-Hv1a (Hv1a) or α-Bungarotoxin (α-Btx) dissolved in phosphate-buffered saline (PBS).

Larval injection of 2.5 nmol/g Hv1a induced locomotor paralysis and full lethality in the control groups (w^{1118}, *THattP40* and *THattP2*, Fig. 2A). Survival was quantified as the percentage of pupae formed after injection. Hv1a failed to achieve full lethality in *nAChRα4* and *nAChRβ2* homozygous mutants, which both showed an increase in survival to 42±22% (One-way ANOVA followed by Bonferroni's test, P=0.0035, Fig. 2A). Mortality in all the other null mutants was comparable to controls (P>0.9).

Next, we observed significant toxicity following injection of 1.25 nmol/g α-Btx. Larvae exhibited a progressive reduction in locomotion until stationary, causing a developmental arrest and, ultimately, death. We found that α-Btx induced lethality is drastically reduced in absence of *nAChRα5*, *nAChRα6* and *nAChRα7*. Survival rate was significantly increased from 0% (controls) to 61±10% (P=0.001), 53±24% (P=0.0051) and 72±25% (One-way ANOVA followed by Bonferroni's test, P=0.0001, Fig. 2B) for the *nAChRα5*, *nAChRα6* and *nAChRα7* null mutants, respectively.

As a further control, injections of PBS alone (vehicle) were performed in parallel. All larvae survived the injection procedure and showed no detectable locomotor defects (Fig. 2A, B).

Altogether, these results demonstrate that Hv1a and α-Btx do not share the same binding pocket and unevenly interact with the different nAChR subunits *in vivo*. Alpha-Btx shows a novel insecticidal effect on nAChRs and therefore we further examined these interactions biochemically.

Forming SMA-lipid particles (SMALPs) of ring-like nAChR complex structures

In order to take advantage of our new receptor subunit mutants for the biochemical analysis of native nAChR functions, we examined the composition of the receptors responsible for binding α-Btx. To address the functionality of *D. melanogaster* nAChRs isolated from endogenous membranes, we utilised detergent-free SMALPs extraction to characterise the interaction between receptor native lipid discs and the α-Btx toxin (Fig. 3A).

In brief, we prepared membrane extracts from adult *D. melanogaster* heads[22] and generated lipid particle discs by solubilising the membrane extracts with the SMA copolymer. We used affinity beads with or without coupling to α-Btx[23,24] to enrich for nAChRs in the SMALP preparations that bound to the toxin, and performed mass spectrometric analysis of tryptic peptides generated from the enriched preparations. In parallel we processed membrane extracts without SMALP and with SMALP extracts enriched with beads alone.

We first determined whether membrane protein discs are formed from enriched membranes using the SMA copolymer. We prepared membrane enriched fractions from adult heads, solubilized these with SMA and separated the insoluble particles from the lipid discs by ultracentrifugation. We negatively stained the SMALP preparations and imaged them with transmission electron microscopy (TEM), observing irregular discs of varying shapes and sizes, with clusters containing different numbers of discs (Fig. 3B).

Membrane receptors often have a unique shape in TEM images and the five subunits of a nAChRs is expected to form a ring-like structure, suggesting that the receptors are extracted as a complex. However, we did not observe pentameric ring-like structures perhaps suggesting that nAChRs are of low abundance and that analysis may benefit from enrichment. We coupled α-Btx to affinity beads to enrich nAChR complexes that bind the toxin in SMALP preparations (Fig. 3C). In contrast to the unenriched samples, TEM images of the enriched preparations showed increased numbers of ring-like structures of 15 nm in diameter (Fig. 3D, E). Thus our TEM analysis shows an increased number of ring-like membrane complexes in the SMALP preparations which are likely to be nAChRs.

Efficient SMALPs extraction allow to study nAChR subunits solubility

To assess to what extent the SMA copolymer solubilized nAChRs, we performed a bottom-up proteomics analysis to identify receptor subunits. Membrane preparations were solubilized in buffer with or without SMA, and affinity beads with or without α-Btx were used to assess ligand-binding to nAChR subunits. Comparing the number of proteins identified in samples solubilized either with or without 5% SMA, we observed a significantly increased identification of proteins dissolved in SMA by equal numbers of MS/MS spectral counts (two-tailed t-test, $P<0.01$, Fig. 4A and non-significant, Fig. 4B). This indicates that mass spectrometer performance was comparable during the measurements.

Sequences of membrane spanning segments of nAChR subunits, which are in close contact to the hydrophobic lipid environment, are largely composed of nonpolar side chains. Determining the average of hydrophobicity scales of identified protein sequences revealed significantly increased numbers of proteins with a positive hydrophobicity score in samples solubilized in SMA (two-tailed t-test, $P<0.0001$, Fig. 4C), indicative of enrichment for membrane proteins. An analysis of Gene Ontology (GO) slim terms supports the conclusion that the SMALP preparations are enriched for membrane embedded and associated proteins (Fig. 4D), and that these are not limited to plasma membrane proteins. In the SMA-enriched samples we found enrichment for proteins annotated with metabolic and catalytic activity terms and also enhanced response to biological stimuli (Supplementary Fig. 1A, B), highlighting the recovery of membrane-associated proteins.

Next, we focused on identified membrane proteins predicted to contain transmembrane helical (TMH) domains and found an increased number of proteins containing TMHs in SMA solubilized samples (Fig. 4E). While the majority of these proteins contained a single TMH domain, we identified Piezo, a mechanosensory ion channel protein containing 37 predicted helices. Both α- and β- subunits of nAChRs contain four TMH domains and could be solubilized in SMA. The number of β-barrel membrane spanning proteins identified was also significantly increased by SMA extraction (two-tailed t-test, $P<0.0001$, Supplementary Fig. 1C).

Furthermore, palmitoylated lipid anchor modifications to nAChR subunits has been shown to be important for receptor assembly into membranes and the formation of functional complexes[25]. Comparing samples solubilized with and without SMA showed a significantly increased identification of proteins which are predicted to be palmitoylated and myristoylated

(two-tailed t-test, $P<0.0001$, Supplementary Fig. 1D, E). In contrast, membrane proteins that are predicted to contain a glycosylphosphatidylinositol (GPI)-anchor are equally solubilized in both conditions (two-tailed t-test, non-significant, Supplementary Fig. 1F).

Focusing on the membrane receptors solubilized by SMA, we analysed the amino acid sequence properties of identified proteins and calculated an overall solubility score[26,27]. Comparing the solubility to the hydrophobicity showed a calculated R^2 of 0.56 (Fig. 4F). Sequences with a score greater than 1 are highly soluble receptors and those less than minus -1 are difficult to solubilize. As a result, samples solubilized in SMA contain more receptors, which are difficult to solubilize. These receptors are more hydrophobic and contain larger numbers of TMH domains (Fig. 4G). Calculating an average solubility score of -2.76 for nAChR sequences indicates that difficult to solubilize subunits are successfully recovered with SMA (Fig. 4H).

Taken together, these analyses confirm that SMA solubilizes nAChR complexes in a state suitable for subunit identification by mass spectrometry and suggests that α-Btx interactions can be studied with SMALP preparations.

Three nAChR α-subunits are targets of α-Btx

To explore native nAChR subunit interactions with α-Btx we searched for peptides from subunit ligand-binding and cytoplasmic domains, identifying the Dα5, Dα6 and Dα7 subunits in the α-Btx affinity bead pull-downs (Fig. 5A, B, Supplementary Table 1). Several other nAChR subunit peptides could be identified in the negative controls performed without coupling α-Btx to affinity beads (Supplementary Table 2). The sequences of the ligand-binding domains of the Dα5, Dα6 and Dα7 subunits are very similar (avg. 95.49 %) and we identified peptides common to all three subunits (Supplementary Fig. 2A) as well as unique peptides within the cytoplasmic domains (Supplementary Fig. 2B). However, we found no peptides mapping to TMH domains. The ligand-binding domain of α-subunits show structural similarity across different species (Supplementary Fig. 3A) and by mapping the identified peptides to known structures we concluded they are most likely outside of the α-Btx binding sites (Supplementary Fig. 3B).

To further characterize the role of the three α-subunits identified in α-Btx binding we generated SMALP preparations and performed α-Btx affinity bead enrichments with adult head

preparations from homozygous null mutations for each of the *nAChRα5*, *nAChRα6* and *nAChRα7* subunit genes. With all three deletion mutants we observed, as expected, no detectable peptides from the missing subunit but could still identify peptides from the other two subunits (Fig. 5C). We compared the repertoire of proteins identified with α-Btx enrichment in wild type with those found in each of the three mutant lines to identify any changes in the representation of biological pathways annotated in KEGG[28] (Fig. 5D). While the enrichments in wild type and the mutants were broadly similar, we noticed a loss of proteins associated with cofactor/vitamin metabolism, particularly retinol and ascorbate, in all three of the mutants as well as proteins associated with vesicular transport. It is possible that these pathway changes represent alterations in neurotransmitter production or trafficking. Interestingly, we also noticed specific enrichment of cytochrome P450 related pathways in the *nAChRα6* mutants, suggesting perturbation of neurotransmitter pathways.

In summary, our analysis indicates that a functional α-Btx binding nAChR involves the Dα5, Dα6 and Dα7 subunits. This is entirely in line with our findings described above, where loss of each of these subunit genes conferred substantial resistance to α-Btx induced lethality.

Glycosylation sites of nAChR subunits by α-Btx binding

We next examined glycosylation sites on nAChR subunits since these are known to have an important role in α-Btx binding affinity in other systems. For example, deglycosylation reduces α-Btx binding in human nAChRs by more than two orders of magnitude[8] and α-Btx binding to loop C in *Torpedo californica* α-subunits is enhanced by N-glycosylation of sites in these regions[20].

To identify specific glycosylation sites in *D. melanogaster* nAChRs we first purified SMALP solubilized receptors with α-Btx affinity beads, digested them into peptides and enriched for glycopeptides using HILIC resin[29] (Fig. 6A). Site-specific identification of glycans on peptides by mass spectrometry is challenging[30] and often requires an additional deglycosylation steps for glycopeptide measurement. Deglycosylation of enriched peptides was carried out using two separate enzymes: Endoglycosidase H (Endo H), which cleaves asparagine-linked oligosaccharides to generate a truncated sugar molecule with one N-acetylhexosamine (HexNAc) residue, .and the endoglycosidase PNGase F, which releases the entire glycan from asparagine residues and deaminates the sugar free asparagine to aspartic acid. While very few

glycopeptides were observed in the flow through (an average 20 glycopeptides Fig. 6B), we identified a total of 397 glycopeptides after enrichment and deglycosylation with Endo H or PNGase F (Fig. 6C).

Shared glycopeptides from Dα5 and Dα7 nAChR subunits were identified after enrichment and deglycosylation with Endo H and PNGase F (Fig. 6D). Deglycosylation with Endo H identified modified asparagine (N2) residues on the peptide (NNGSCLYVPPGIFK), which is predicted to be part of the Dα5 and Dα7 ligand-binding domains involved in α-Btx binding. This asparagine residue was modified with an N-acetylhexosamine (HexNAc) truncated sugar chain. Releasing N-glycans after deglycosylation by PNGase F enabled us to identify a deaminated asparagine residue in the same peptide. The monoisotopic mass of this peptide changed due to the different modifications on the asparagine residue (Fig. 6E).

The genome of *Caenorhabditis elegans* encodes for at least 29 nAChR subunits[31]. The alpha-type unc-63 subunit contains an N-linked HexNAc modified asparagine residue on position 136[32]. Performing a multiple sequence alignment showed that this asparagine residue is conserved between insects and nematodes (Supplementary Fig. 4A). Comparing identified glycosylation sites of Dα5 and Dα7 subunits to known N-linked glycosylation sites of α-subunits from *T. californica*, *Danio rerio*, *Mus musculus* or *Homo sapiens* indicates that this site is not conserved between vertebrates and invertebrates (Supplementary Fig. 4B).

We also identified glycosylation sites in the Dα3 (ATKATLNYTGR) and Dβ3 (VVLPENGTAR) subunits after Endo H treatment but not with PNGase F treatment, suggesting they harbour a single N-linked HexNAc modified asparagine residue (Supplementary Fig. 4C).

Taken together these findings suggest that the Dα5 and Dα7 subunits are modified on asparagine residues in the α-Btx ligand-binding domain with an N-linked sugar chain.

Localization of Dα6 nAChRs subunit in the brain

In order to examine the endogenous localization of an α-Btx binding receptor subunit we used CRISPR/Cas9 genome engineering to introduce in frame C-terminal fluorescence and epitope tags into the endogenous *nAChRα6* locus. The resulting line is homozygous viable and fertile, and shows no apparent phenotypes. We live imaged the unfixed brains of larvae and adults

homozygous for the tagged line using confocal microscopy. In 2nd instar larvae we observed low level well-distributed fluorescence signal throughout the ventral nerve cord (VNC), including on commissural axons, and in the developing brain (Fig. 7A). By early L3, we found more defined localization in the VNC and developing mushroom bodies (Fig. 7B), particularly noticeable in the Kenyon cells, a known site of α-Btx binding[33]. Localization in larval mushroom bodies continued to evolve, with defined expression in the Kenyon cells, calyx, peduncle, dorsal and medial lobes as well as the medulla and lamina of the emerging optic lobes (Fig. 7C, E). We also observed localisation to a number of cell bodies overlying the optic lobes (Fig. 7F). Finally, in the adult brain, expression was largely restricted to the mushroom bodies particularly the Kenyon cells and connections across the midline between the β and γ lobes and the optic lobes (Fig. 7G). The temporal localization of Dα6 subunit in the CNS is summarized in schematic form (Fig. 7H).

Discussion

Elucidation of complex insect nAChRs heterogeneity will lead to a better understanding of selective insecticidal effects. We present a new set of null mutations in all *D. melanogaster nAChR* subunit genes and investigated insecticidal peptide toxin effects on insect larvae. Utilising biochemical approaches with SMALP pull-downs we characterised toxin binding and subunit composition of native nAChR complexes.

Our genome engineering approach generated viable and fertile mutations in nine out of the ten subunit genes encoded in the *D. melanogaster* genome and is largely concordant with the recently described work by Perry and colleagues[2]. In both studies, null mutations in the *nAChRβ1* gene were inviable as stocks. We add to the previous work by generating viable mutations in *nAChRα5*. We observed some minor morphological defects in some of the null mutants especially in *nAChRα1*, *nAChRα2*, *nAChRα3*, *nAChRα5* and *nAChRβ3* as well as locomotor defects with some alleles, particularly severely in *nAChRα3* homozygotes and *nAChRβ1* heterozygotes. Locomotor defects are in agreement with previously reported neuronal phenotypes with *nAChR* subunit genes, including sleep disruption, defective jump response, memory impairment or locomotor defects[21,34,35,36].

We used the nAChR null mutants to study insecticidal effects of the Hv1a peptide on viability after injection into larvae and investigated whatever α-Btx has any insecticidal properties. As

described by Chambers and colleagues, we confirm that Hv1a effects nAChRs[5] and our analysis shows that the Dα4 and Dβ2 subunits are involved in the insecticidal response. We show for the first time that α-Btx has selective insecticidal effects against the Dα5, Dα6 and Dα7 subunits, which we further characterized at the biochemical level.

The pharmacology of Hv1a and α-Btx binding has been shown to be distinctive[5], correlating with our demonstration that these two peptide toxins mediate their effects through different receptor alpha subunits. Furthermore, resistance to neonicotinoid insecticides, which interact most strongly with Hv1a binding, has been associated with Dβ2[2,37], consistent with the involvement of this subunit in the response to Hv1a. However, no resistance to neonicotinoids was seen in *D. melanogaster* having a deletion in Dα4[2], which could be explained if neonicotinoids act at multiple receptor classes. Multiple binding sites for the neonicotinoid imidacloprid can be resolved in equilibrium binding assays in many insect species[38] and by binding kinetics in flies[39].

Resistance to spinosad is strongly associated with Dα6[2], and spinosad binding is much more sensitive to the action of α-Btx than to the action of neonicotinoids[5], again consistent with the involvement of this subunit with sensitivity to injected α-Btx and with the proposition that α-Btx and Hv1a act at distinct receptor classes.

nAChR subunits are known to be difficult to purify due to solubilisation issues[40,41] and the requirement for a lipid environment for ligand binding[12] makes it challenging to study these receptors in native conditions. We used the SMALPs extraction method for preparing membrane discs and enriched nAChRs via α-Btx affinity purification. Electron microscopy analysis indicated that receptor-like particles were recovered and these were substantially enriched by α-Btx pull-down. Mass spectrometry analysis showed an enrichment for the Dα5, Dα6 and Dα7 subunits in these preparations, which is concordant with our *in vivo* injection results and previous studies that characterised aspects of α-Btx binding[,10,11,42].

To our knowledge this is the first report of the identification of a native endogenous α-Btx binding nAChRs. We note however, that we cannot determine from our analysis whether all three identified subunits are part of the same complex or if there are different receptors containing a subset of these subunits. Using chimeric receptors in a cell line system, Landsdell and colleagues reported that a combination of all three of these subunits show high affinity acetylcholine binding but α-Btx binding varied depending on receptor combinations, with Dα5 and Dα6 binding most strongly[11]. In a prior study they implicated Dα6 and Dα7[10]. However,

these assays were performed with 5HT3A-nAChR subunit fusions, here we provide strong evidence that these three subunits bind to α-Btx *in vitro* and *in vivo*.

In addition, glycopeptide enrichment showed site specific glycosylation modifications on the Dα5 and Dα7 nAChR subunit ligand binding domains. The unique lipid environment and glycosylation sites of nAChR α-subunits from the electric ray, *T. californica,* were found to be important for α-Btx binding activities[43,20], and structural studies support this conclusion[8]. Our work supports the view that there is a role for Dα5 and Dα7 glycosylation modifications in the recognition of α-Btx in *D. melanogaster*.

Our localization studies with fluorescence tagged endogenous Dα6 subunit showed relatively restricted expression in the brain and ventral nerve cord, with prominent expression in the Kenyon cells of the mushroom body, all known regions. The expression of Dα6 in Kenyon cells across development is in line with a proposed role for this subunit in memory plasticity, along with other α-subunits including Dα5, in mushroom body output neurons[44]. Thus, it is possible that retention of α-Btx binding in the absence of Dα6 may simply reflect its restricted localisation. In contrast, it is clear that Dα6 plays a major and specific role in binding to the insecticide spinosad in *D. melanogaster* since mutations in this subunit are highly resistant to the toxin [45].

Localization studies of Dα6 nAChRs subunit fusion protein by confocal microscopy are largely consistent with recent reports of *nAChRα6* expression derived from expression reporters[46], though these studies appear to indicate wider adult brain expression than we observed, perhaps reflecting a degree of translational control or limitations in the sensitivity of our live imaging.

In conclusion, we identified ligand-binding subunit sites for a *D. melanogaster* nAChR antagonist with newly insecticidal effects. Our findings contribute to a better understanding of the role of nAChR subunits which interacts with insecticidal peptide toxins.

Materials and methods

Drosophila methods

Embryos were injected using standard procedures into the *THattP40* or *THattP2* lines expressing *nos*-Cas9. Donor DNA (500 ng/μL) in sterile dH_2O was injected together with of gRNA plasmids (100 ng/μL) as described previously[47]. Individually selected surviving adults were crossed to w^{1118} and the progeny screened for DsRED fluorescence localized mostly to the eyes of transgenic flies: positive flies were balanced and homozygous stocks established where possible. The correct localization of the insert was confirmed via PCR and sequencing. Transgenic flies were assessed for the phenotype using bright field microscope. For tagging of *nAChRα6*, the stocks were additionally subjected to Cre-recombination for marker removal and several independent lines were verified by PCR. Some of these lines were screened for YFP fluorescence using confocal microscopy. From the YFP positive balanced stocks, the viable and fertile homozygote was established. Injections were performed by the Department of Genetics Fly Facility (https://www.flyfacility.gen.cam.ac.uk). All fly stocks were maintained at 25℃ on standard cornmeal medium. Larvae of 2nd and 3rd stage were collected, and their brains were dissected according to standard protocols. Brains were mounted in glycerol and live imaged.

Cloning of gRNAs and generation of donor vectors

Construction of *nAChR* subunits null alleles

In order to generate individual *nAChR* subunits gene deletions the open reading frame (ORF) was disrupted by introducing a visible marker harbouring DsRED marker under eye specific driver 3Px3 using CRISPR/Cas9 technology as previously described[47]. The targeted exons are shared between different isoforms and adjacent to the N-terminus to ensure the protein translated was interrupted. The insertion sites were designed *in silico* and optimal gRNAs were chosen (Supplementary Table 3) that were tested against the injection strain and cloned into pCDF3. Briefly, target specific sequences were synthesized and either 5′-phosphorylated annealed and ligated into the *Bbs*I sites of pCDF3 precut with *Bbs*I. Positive clones were confirmed by sequencing.

For generation of donor vectors, firstly, homology arms were amplified on genomic DNA (Supplementary Table 4) that, secondly, were used as a template to amplify the homology arms (Supplementary Table 5) of the donor vector for CRISPR/Cas9 homologous recombination (HDR). The inserts with visible marker were amplified using as a template previously generated constructs[47] with appropriate primers. These fragments were used for Gibson assembly using Gibson Assembly Master Mix (New England Biolabs). PCR products were produced with the Q5 High-Fidelity 2X Master Mix (New England Biolabs). All inserts were verified by sequencing.

C-terminal tagging of Dα6 nAChRs subunit fusion protein

For tagging of Dα6 nAChRs subunit the C-terminal fusion with FSVS fluorescent protein harbouring StrepII and 3xFLAG epitope tags (3xFLAG-StrepII-Venus-StrepII) was generated for CRISPR/Cas9 mediated genome engineering[47,48]. Firstly, gRNAs were designed (Supplementary Table 3) and tested against the genomic DNA sequence of injection strains. The oligos were phosphorylated and ligated into *Bbs*I precut pCDF3. The positive variants were confirmed by sequencing.

The donor vector to generate protein fusion with fluorescent protein harbouring epitope tags was cloned in 2 steps strategy by creating initially (A) nAChRα6-FSVS donor and then adding the removable marker to generate (B) nAChRα6-FSVS-loxP-3PX3_DsRED_loxP donor vector. At first, the homology arms were enriched on genomic DNA (Supplementary Table 4) and used to amplify homology arms for donor vector nAChRα6-FSVS (Supplementary Table 5) that was assembled using Gibson Assembly as described above. The FSVS tag was amplified on previously generated constructs[48] with appropriate overlapping oligos (Supplementary Table 5). The construct was confirmed by Sanger sequencing and used as a template to generate donor vector with removable marker. The PCR fragments harbouring homology arms and FSVS tag were amplified on nAChRα6-FSVS construct, whereas the 3PX3-DsRed with adjacent loxP sites was amplified using earlier generated constructs[48]. The final donor vector was generated using Gibson Assembly® as described above and positive variants were confirmed by sequencing.

Confocal microscopy

Localization of FSVS-tagged (3xFLAG-StrepII-Venus-StrepII) Dα6 nAChRs subunit was visualised in dissected larvae brains via monitoring the YFP fluorescence (Venus). Briefly, the larval brains were dissected and mounted in glycerol for live imaging. Images were acquired using a Leica SP8 confocal microscope (Leica microsystems) with appropriate spectral windows for mVenus, images were processed with the Fiji software.

Locomotor behaviour

Adult female and male flies were collected shortly after eclosion and separated into 10 cohorts consisting of 10 flies (100 total) for each genotype (Supplementary Table 6). Flies were maintained at 25°C and transferred to fresh food every three days. For the climbing assay, each cohort was transferred to 10ml serological pipette, and allowed to acclimatize for five min. For each trial, flies were tapped down to the bottom of the vial, and the percentage of flies able to cross a five-ml mark successfully within 10 seconds was recorded as the climbing index. Five trials were performed for each cohort, with a 1-min recovery period between each trial. Climbing assays were performed 10 days after eclosion.

Drosophila larval injections

Injections were performed by using the Nanoliter 2000 (World Precision Instruments, Hertfordshire, UK) mounted on a micromanipulator (Narishige, London, United Kingdom). Micropipettes were pulled from glass capillary tubes (1.14 mm OD, 0.530 mm ± 25 µm ID; #4878, WPI) using a laser-based micropipette puller (Sutter P-2000, Sutter Instrument, Novato, CA, USA). Third instar larvae (wandering stage) were transferred to an adhesive surface after being quickly washed with water to remove food residues and gently dried using paper tissue. The micropipette was positioned over the approximate centre of the body, on the dorsal side, and the tip was advanced through the cuticle into the hemocoel of the larva. Larvae were injected with 69 nL of PBS supplemented with 10% (v/v) filtered food dye (PME, moss green food colouring; 0.2 µm filter). Food dye was included to aid in monitoring the success of the injection under a dissection microscope (Leica MZ65, Milton Keynes, United Kingdom). ω-hexatoxin-Hv1a (Hv1a, Syngenta, Schaffhauserstrasse, CH-4332 Stein, Switzerland) and α-

Bungarotoxin (α-Btx, Abcam, Cambridge, United Kingdom, ab120542) were added to the injection mix in order to obtain a final concentration of 2.5 nmol/g and 1.25 nmol/g, respectively (average larval weight was 2.14 mg). After injection, larvae were then gently transferred into agar/grape juice (Ritchie Products Limited, Burton-On-Trent, United Kingdom) plates and kept at 25°C. The rate of survival (expressed as percentage) was calculated as the number of living pupae, formed 1-2 days after injection, divided by the total number of injected larvae. Experiments were repeated three times independently with a total number of 10 larvae for each experimental group (Supplementary Table 7). Results were analysed with One-way ANOVA followed by Bonferroni's multiple comparisons test using GraphPad Prism (version 7, GraphPad Software, San Diego, California, USA).

Coupling procedure of α-bungarotoxin to affinity beads

Coupling of α-bungarotoxin, α-Btx (Abcam, Cambridge, United Kingdom, ab120542) to cyanogen bromide-activated (CNBr) sepharose beads 4B (Sigma-Aldrich, Haverhill, United Kingdom, C9 142-5G) was performed as described[23,24]. CNBr-activated sepharose 4B beads (0.25 g) were hydrated in 1.25 ml of 1 mM HCl for 1 hr at 4°C on a rotator. Beads were centrifuged for 5 min at 1500 × g, the supernatant removed and beads washed twice with 1 ml of coupling buffer (0.25 M $NaHCO_3$, 0.5 M NaCl, pH 8.3). Beads were centrifuged for 5 min at 1500 × g and the supernatant was removed. Alpha-Btx (1 mg) was resuspended in 1 ml coupling buffer and incubated together with the affinity beads at 4°C for 16 hr on a rotator. Beads were centrifuged for 5 min at 1500 × g. Coupling efficiency was determined using a Pierce quantitative fluorometric peptide kit and used according to the manufacturer's instructions (Thermo Scientific™, Bishop's Stortford, United Kingdom, 23290). Beads were blocked with 1 ml of 0.2 M glycine in 80 % coupling buffer at 4°C for 16 hr on a rotator. Beads were then centrifuged for 5 min at 1500 × g and washed with 1 ml of 0.1 M $NaHCO_3$, 0.5 M NaCl, pH 8.0. This step was repeated with 1 ml of 0.1 M $NaCH_3CO_2$, 0.5 M NaCl, pH 4.0. Beads were washed again in 1 ml of 0.1 M $NaHCO_3$, 0.5 M NaCl, pH 8.0. After a final wash step with 1 ml coupling buffer the beads were incubated twice for 30 min in 1 ml Tris-buffer (50 mM Tris, 150 mM NaCl, pH 8.0). The beads were centrifuged for 5 min at 1500 × g, the supernatant was removed and 20 µl TBS, pH 8.0 was added.

Membrane protein enrichment and incorporation in SMALPs

D. melanogaster heads were obtained and separated according to[22]. In a 50 ml falcon tube approximately 6 g flies were rapidly frozen in liquid nitrogen and vortexed twice for 3 min, with the tube cooled for 30 sec in liquid nitrogen between. Heads were separated from bodies by sieving (Endecotts, London, United Kingdom, 1201124 & 1201125). 1 ml of isotonic lysis buffer (0.25 M sucrose, 50 mM TRIS/HCl pH 7.4, 10 mM HEPES pH 7.4, 2mM EDTA, Protease inhibitor) was added to approximately 0.8 g separated heads. The solution was mixed three times by vortexing and the heads were lysed with 60 strokes in a dounce homogenizer with a pestle. Membrane protein preparation was performed by differential centrifugation-based fractionation as described[22,49]. Membrane protein pellets were resuspended in 20 to 100 µl 5 % SMALP solution (5 % styrene maleic acid copolymer (3:1), 5 mM Tris-Base, 0.15 mM NaCl, pH 8.0). For efficient incorporation and formation of SMALPs, membrane proteins were incubated with 5 % SMALP solution for 2 hr at room temperature on a rocking platform. To separate the insoluble proteins from the soluble SMALPs a centrifugation step at 100,000 × g for 60 min, 4°C was performed. Supernatant containing the SMALPs were combined and used for the nAChRs pull-downs.

Enrichment of nAChRs by α-Btx pull-down

SMALPs (20-35 mg/ml) were incubated with 200 µl α-Btx conjugated affinity beads for 16 hr, 4°C on a rotator. The beads were then centrifuged for 5 min at 1500 × g and washed two or three times, each for 10 min with 1 ml ice-cold TBS (50 mM Tris, 150 mM NaCl, pH 8.0) on a rotator at 4°C. Beads were centrifuged for 5 min at 1500 × g and nAChRs selectively eluted twice with 100 µl 1 M carbachol (Insight Biotechnlogy Ltd, Wembley, United Kingdom, CAS 51-83-2). These steps were performed for 25 min at room temperature on a rotator. Beads were centrifuged for 5 min at 1500 × g and eluates were combined and ice-cold 100 % acetone in the volume of four times of the sample was added to the samples, mixed by vortexing and proteins were precipitated for 16 hr at -20°C. Samples were centrifuged at 13000 × g for 15 min. Supernatant was removed and dried proteins were dissolved in Laemmli buffer (1M Tris pH 6.8, 10 % SDS, 5 % glycerol, 2 % bromophenol blue). Proteins were heated at 60°C and loaded on mini-protean tgx precast gel (4-15 %, Bio-Rad Laboratories, Inc., Watford, United Kingdom, catalogue # 456–1084).

Electron microscopy preparation

For negative staining analysis, membrane proteins were extracted with 5 % SMA and nAChRs were enriched using α-Btx affinity pull-downs. Proteins were diluted 1:10 with deionised water to approximately 0.9 mg/ml and an aliquot of the samples were absorbed onto a glow-discharged copper/carbon-film grid (EM Resolutions) for approximately 2 min at room temperature. Grids were rinsed twice in deionised water and negative staining was performed using a 2 % aqueous uranyl acetate solution. Samples were viewed in a Tecnai G2 transmission electron microscope (TEM, FEI/ThermoFisher) run at 200 keV accelerating voltage using a 20 μm objective aperture to increase contrast; images were captured using an AMT CCD camera.

Sample preparation for liquid chromatography–mass spectrometry (LC-MS)

The protein lanes were excised from the gels and proteolytic digestion with trypsin/lys-C mix (Promega, Southampton, United Kingdom, V5073) was performed as described[50]. The gel pieces were covered with 50 mM NH_4HCO_3 / 50 % ACN and shaken for 10 min. This step was repeated with 100 % acetonitrile and finally dried in a speed vac. Samples were reduced with 10 mM DTT in 50 mM NH_4HCO_3 at 56°C for 1 hr and alkylated with 50 mM iodoacetamide in 50mM NH_4HCO_3 at room temperature without light for 45 min. The gels were covered with 50 mM NH_4HCO_3 and 100 % ACN and shaken for 10 min. These steps were repeated and samples were dried in a speed vac. Trypsin/lys-C burffer was added to the sample according to manufacturer's instructions and incubated for 45 min on ice. Next 30 μl 25 mM NH_4HCO_3 was added and samples were incubated at 37°C for 16 hr. The gel pieces were covered with 20 mM NH_4HCO_3 and shaken for 10 min. Supernatant with peptides was collected. Next, the gels were covered with 50 % ACN / 5 % FA and shaken for 20 min. These steps were repeated and peptides were dried in a speed vac. Samples for glycopeptide enrichment were digested in-solution according to[51]. Samples were reduced and alkylated in 10 mM DTT and 50 mM iodoacetamide. Proteins were digested in final concentration of 2.5 μg trypsin/lys-C buffer for 16 hr at 37°C.

Peptide clean-up

Peptides were desalted using C-18 stage tips according to[52]. C-18 material (three C-18 plugs were pasted in a 200 µl pipette tip, Pierce™ C18 Spin Tips, Thermo Scientific™, Bishop's Stortford, United Kingdom, 84850) was equilibrated with methanol/0.1 % FA , 70 % ACN/0.1 % FA and with 0.1 % FA. Peptides were loaded on C-18 material, washed with 0.1 % FA and eluted with 70 % ACN/0.1 % FA. Samples were dried and finally, peptides were resuspended in 20 µl 0.1 % FA. For glycopeptide enrichment peptides were first desalted using poros oligo r3 resin (Thermo Scientific™, Bishop's Stortford, United Kingdom, 1-339-09) as described[51,53]. Pierce™ centrifuge columns (Thermo Scientific™, Bishop's Stortford, United Kingdom, SH253723) were filed with 250 µl of poros oligo r3 resin. Columns were washed three times with 0.1 % TFA. Peptides were loaded onto the columns and washed three times with 0.1 % TFA and subsequently eluted with 70 % ACN.

Glycopeptide enrichment

Enrichment of glycopeptides of nAChRs was performed as described[29]. Micro columns were prepared with 200 µl peptide tips filled with a C8 plug and iHILIC – fusion 5µm, 100 Å silica based material (Hilicon, Umeå, Sweden, HCS 160119). Peptides were solubilized stepwise in 19 µl dH_2O and then in 80 µl ACN plus 1 µl TFA acid. The micro columns were cleaned with 50 µl 0.1 % TFA and three times equilibrated with 100 µl 80 % ACN, 1 % TFA. Peptides were loaded onto the micro column and washed twice with 100 µl 80 % ACN, 1 % TFA. Glycopeptides were eluted from the column using twice 40 µl 0.1 % TFA and finally with 20 µl 80 % ACN, 1 % TFA. Samples were dried in a speed vac before peptides were deglycosylated with Endo H or PNGase F according to manufacturer's instructions (New England Biolabs Inc., Hitchin, United Kingdom, P07025 & P0710S).

LC-MS/MS

Peptide samples were dissolved in 20 µl of 0.1 % (v/v) FA. Approximately 1 µg peptide solution was used for each LC-MS/MS analysis. All LC-MS/MS experiments were performed using a Dionex Ultimate 3000 RSLC nanoUPLC (Thermo Fisher Scientific Inc, Waltham, MA, USA) system and a Q Exactive™ Orbitrap mass spectrometer (Thermo Fisher Scientific Inc, Waltham, MA, USA). Separation of peptides was performed by reverse-phase chromatography at a flow rate of 300 nL/min and a Thermo Scientific reverse-phase nano Easy-spray column (Thermo Scientific PepMap C18, 2µm particle size, 100A pore size, 75 µm i.d. x 50 cm length). Peptides were loaded onto a pre-column (Thermo Scientific PepMap 100 C18, 5µm particle size, 100A pore size, 300 µm i.d. x 5mm length) from the Ultimate 3000 autosampler with 0.1 % FA for 3 min at a flow rate of 15 µL/min. After this period, the column valve was switched to allow elution of peptides from the pre-column onto the analytical column. Solvent A was water + 0.1 % FA and solvent B was 80 % ACN, 20 % water + 0.1 % FA. The linear gradient employed was 2-40 % B in 90 min (the total run time including column washing and re-equilibration was 120 min). In between runs columns were washed at least four times to avoid any carryovers. The LC eluant was sprayed into the mass spectrometer by means of an Easy-spray source (Thermo Fisher Scientific Inc.). An electrospray voltage of 2.1 kV was applied in order to ionize the eluant. All *m/z* values of eluting ions were measured in an Orbitrap mass analyzer, set at a resolution of 35000 and scanned between *m/z* 380-1500 Data dependent scans (Top 20) were employed to automatically isolate and generate fragment ions by higher energy collisional dissociation (HCD, Normalised collision energy (NCE): 25 %) in the HCD collision cell and measurement of the resulting fragment ions were performed in the Orbitrap analyser, set at a resolution of 17500. Singly charged ions and ions with unassigned charge states were excluded from being selected for MS/MS and a dynamic exclusion of 20 seconds was employed.

Peptide/protein database searching

Protein identification was carried out using mascot or sequest HT search engine software operating in Proteome Discoverer 2.3[54,55]. Raw flies were searched against the uniprot *Drosophila_melanogaster*_20180813 database (23297 sequences; 16110808 residues) and a common contaminant sequences database. The search parameters using mascot algorithm were: (i) trypsin was set as the enzyme of choice, (ii) precursor ion mass tolerance 20 ppm, (iii)

fragment ion mass tolerance 0.1 Da, (iv) maximum of two missed cleavage sites were set, (v) a minimum peptide length of six amino acids were set, (vi) fixed cysteine static modification by carbamidomethylation, (vii) variable modification by methionine oxidation & deamidation on asparagine and glutamine and N-acetylhexosamine (HexNAc(1)dHex(1) + HexNAc on asparagine) as variable glycopeptide modifications, (viii) A site probability threshold of 75 % was set, (ix) Percolator was used to assess the false discovery rate and peptide filters were set to high confidence (FDR<1).

Data handling and statistical analysis

Protein data evaluation was performed using R 3.5.3[56]. Plotting was performed in RStudio 1.3.959[57] using ggplot2[58] and other R packages. In order to characterise membrane proteins the following tools were used: (i) TMHMM - 2.0[59], (ii) PRED-TMBB2[60] (iii) SwissPalm[61], (iv) PredGPI[62], (v) Gravy calculator (www.gravy-calculator.de), (vi) Myristoylator[63] (vii) Solubility scores[26,27]. Analysis of gene ontology (GO) slim terms[64] were performed within proteome discoverer 2.3 (Thermo Fisher Scientific). KEGG[28] pathway enrichment analysis was performed using DAVID[65]. For each experimental investigation $n \geq 3$ were considered and data are represented as means ± SEM. Experiments were performed in a blinded manner whenever possible. Data are presented as mean ± SD. Statistical tests for SMALPs were performed using two-tailed t-test with an unequal variance and *P* values of ≤ 0.05 were considered to be significant. In DAVID, Fisher's exact *P* values are computed to measure the gene-enrichment terms. Fisher's exact *P* value of 0 represents perfect enrichment of a term. Usually *P* value of ≤ 0.05 are to be considered as strongly enriched. In this study the default threshold set in DAVID of 0.1 was used. Linear regression analysis was performed in order to study the efficiency of SMALPs extraction of membrane receptors.

Structural assessment and illustration of nAChR subunits

For structural alignment of nAChRs matchmaker command operating in UCSF Chimera X 0.91[66] was used. This command is superimposing protein structures by first creating pairwise sequence alignments, then fitting the aligned residue pairs and displays in an overlaid structure as a result. The following parameters were set to create the aligned structure: (i) alignment algorithm; Needleman-Wunsch (ii) similarity matrix; BLOSUM-62. Structural animation was

performed in Blender 2.8 (www.blender.org), an open-source 3D graphics software. For annotation of protein sequences InterProScan was used[67]. Illustrator for biological sequences (IBS) web server was used to present biological sequences[68]. Multiple sequence alignments were performed[69] or using BoxShade multiple sequence alignments (Swiss institute of bioinformatics).

Reference

1. Ihara, M. *et al.* Cofactor-enabled functional expression of fruit fly, honeybee, and bumblebee nicotinic receptors reveals picomolar neonicotinoid actions. *Proc. Natl. Acad. Sci. U. S. A.* (2020). doi:10.1073/pnas.2003667117

2. Perry, T. *et al.* Role of nicotinic acetylcholine receptor subunits in the mode of action of neonicotinoid, sulfoximine and spinosyn insecticides in Drosophila melanogaster. *Insect Biochem. Mol. Biol.* (2021). doi:10.1016/j.ibmb.2021.103547

3. Zuo, Y. Y. *et al.* Knockin of the G275E mutation of the nicotinic acetylcholine receptor (nAChR) α6 confers high levels of resistance to spinosyns in Spodoptera exigua. *Insect Sci.* (2021). doi:10.1111/1744-7917.12922

4. Salgado, V. L. Selective actions of insecticides on desensitizing and non-desensitizing nicotinic acetylcholine receptors in cockroach (Periplaneta americana) neurons. *Pest Manag. Sci.* (2021). doi:10.1002/ps.6396

5. Chambers, C. *et al.* Insecticidal spider toxins are high affinity positive allosteric modulators of the nicotinic acetylcholine receptor. *FEBS Lett.* (2019). doi:10.1002/1873-3468.13435

6. Houchat, J. N. *et al.* Mode of action of sulfoxaflor on α-bungarotoxin-insensitive nAChR1 and nAChR2 subtypes: Inhibitory effect of imidacloprid. *Neurotoxicology* (2019). doi:10.1016/j.neuro.2019.06.003

7. Dacosta, C. J. B., Free, C. R. & Sine, S. M. Stoichiometry for α-bungarotoxin block of α7 acetylcholine receptors. *Nat. Commun.* (2015). doi:10.1038/ncomms9057

8. Dellisanti, C. D., Yao, Y., Stroud, J. C., Wang, Z. Z. & Chen, L. Crystal structure of the extracellular domain of nAChR α1 bound to α-bungarotoxin at 1.94 Å resolution. *Nat. Neurosci.* (2007). doi:10.1038/nn1942

9. Schmidt-Nielsen, B. K., Gepner, J. I., Teng, N. N. H. & Hall, L. M.

CHARACTERIZATION OF AN α-BUNGAROTOXIN BINDING COMPONENT FROM DROSOPHILA MELANOGASTER. *J. Neurochem.* (1977). doi:10.1111/j.1471-4159.1977.tb06505.x

10. Lansdell, S. J. & Millar, N. S. Molecular characterization of Dα6 and Dα7 nicotinic acetylcholine receptor subunits from Drosophila: Formation of a high-affinity α-bungarotoxin binding site revealed by expression of subunit chimeras. *J. Neurochem.* (2004). doi:10.1111/j.1471-4159.2004.02499.x

11. Lansdell, S. J., Collins, T., Goodchild, J. & Millar, N. S. The Drosophila nicotinic acetylcholine receptor subunits Dα5 and Dα7 form functional homomeric and heteromeric ion channels. *BMC Neurosci.* (2012). doi:10.1186/1471-2202-13-73

12. Dacosta, C. J. B., Dey, L., Therien, J. P. D. & Baenziger, J. E. A distinct mechanism for activating uncoupled nicotinic acetylcholine receptors. *Nat. Chem. Biol.* (2013). doi:10.1038/nchembio.1338

13. Denisov, I. G. & Sligar, S. G. Nanodiscs for structural and functional studies of membrane proteins. *Nature Structural and Molecular Biology* (2016). doi:10.1038/nsmb.3195

14. Loo, R. R., Dales, N. & Andrews, P. C. The effect of detergents on proteins analyzed by electrospray ionization. *Methods Mol. Biol.* (1996).

15. Lee, S. C. *et al.* A method for detergent-free isolation of membrane proteins in their local lipid environment. *Nat. Protoc.* (2016). doi:10.1038/nprot.2016.070

16. Gault, J. *et al.* Combining native and 'omics' mass spectrometry to identify endogenous ligands bound to membrane proteins. *Nat. Methods* (2020). doi:10.1038/s41592-020-0821-0

17. Martens, C. *et al.* Direct protein-lipid interactions shape the conformational landscape of secondary transporters. *Nat. Commun.* (2018). doi:10.1038/s41467-018-06704-1

18. Kalxdorf, M. *et al.* Cell surface thermal proteome profiling tracks perturbations and drug targets on the plasma membrane. *Nat. Methods* (2021). doi:10.1038/s41592-020-01022-1

19. Sobotzki, N. *et al.* HATRIC-based identification of receptors for orphan ligands. *Nat. Commun.* (2018). doi:10.1038/s41467-018-03936-z

20. Rahman, M. M. *et al.* Structure of the Native Muscle-type Nicotinic Receptor and Inhibition by Snake Venom Toxins. *Neuron* (2020). doi:10.1016/j.neuron.2020.03.012

21. Somers, J., Luong, H. N. B., Mitchell, J., Batterham, P. & Perry, T. Pleiotropic effects of loss of the Dα1 subunit in Drosophila melanogaster: Implications for insecticide resistance. *Genetics* (2017). doi:10.1534/genetics.116.195750

22. Depner, H., Lützkendorf, J., Babkir, H. A., Sigrist, S. J. & Holt, M. G. Differential centrifugation-based biochemical fractionation of the Drosophila adult CNS. *Nat. Protoc.* (2014). doi:10.1038/nprot.2014.192

23. Mulcahy, M. J., Paulo, J. A. & Hawrot, E. Proteomic Investigation of Murine Neuronal α7-Nicotinic Acetylcholine Receptor Interacting Proteins. *J. Proteome Res.* (2018). doi:10.1021/acs.jproteome.8b00618

24. Wang, H. *et al.* Nicotinic acetylcholine receptor α7 subunit is an essential regulator of inflammation. *Nature* (2003). doi:10.1038/nature01339

25. Alexander, J. K. *et al.* Palmitoylation of nicotinic acetylcholine receptors. in *Journal of Molecular Neuroscience* (2010). doi:10.1007/s12031-009-9246-z

26. Sormanni, P., Amery, L., Ekizoglou, S., Vendruscolo, M. & Popovic, B. Rapid and accurate in silico solubility screening of a monoclonal antibody library. *Sci. Rep.* (2017). doi:10.1038/s41598-017-07800-w

27. Sormanni, P., Aprile, F. A. & Vendruscolo, M. The CamSol method of rational design of protein mutants with enhanced solubility. *J. Mol. Biol.* (2015). doi:10.1016/j.jmb.2014.09.026

28. Kanehisa, M., Furumichi, M., Sato, Y., Ishiguro-Watanabe, M. & Tanabe, M. KEGG: integrating viruses and cellular organisms. *Nucleic Acids Res.* (2020). doi:10.1093/nar/gkaa970

29. Hägglund, P., Bunkenborg, J., Elortza, F., Jensen, O. N. & Roepstorff, P. A new strategy for identification of N-glycosylated proteins and unambiguous assignment of their glycosylation sites using HILIC enrichment and partial deglycosylation. *J. Proteome Res.* (2004). doi:10.1021/pr034112b

30. Fang, P. *et al.* A streamlined pipeline for multiplexed quantitative site-specific N-glycoproteomics. *Nat. Commun.* (2020). doi:10.1038/s41467-020-19052-w

31. Jones, A. K., Davis, P., Hodgkin, J. & Sattelle, D. B. The nicotinic acetylcholine receptor gene family of the nematode Caenorhabditis elegans: An update on nomenclature. *Invertebr. Neurosci.* (2007). doi:10.1007/s10158-007-0049-z

32. Kaji, H. *et al.* Proteomics reveals n-linked glycoprotein diversity in Caenorhabditis elegans and suggests an atypical translocation mechanism for integral membrane proteins. *Mol. Cell. Proteomics* (2007). doi:10.1074/mcp.M600392-MCP200

33. Su, H. & O'Dowd, D. K. Fast synaptic currents in Drosophila mushroom body kenyon cells are mediated by α-bungarotoxin-sensitive nicotinic acetylcholine receptors and picrotoxin-sensitive GABA receptors. *J. Neurosci.* (2003). doi:10.1523/jneurosci.23-27-09246.2003

34. Fayyazuddin, A., Zaheer, M., Hiesinger, P. R. & Bellen, H. The Nicotinic Acetylcholine Receptor Dα7 Is Required for an Escape Behavior inDrosophila. *PLoS Biol.* (2006). doi:10.1371/journal.pbio.0040063.sg002

35. Tackenberg, M. C. *et al.* Neonicotinoids disrupt circadian rhythms and sleep in honey bees. *Sci. Rep.* (2020). doi:10.1038/s41598-020-72041-3

36. Rohde, P. D. *et al.* Testing candidate genes for attention-deficit/hyperactivity disorder in fruit flies using a high throughput assay for complex behavior. *Fly (Austin).* (2016). doi:10.1080/19336934.2016.1158365

37. Perry, T., Heckel, D. G., McKenzie, J. A. & Batterham, P. Mutations in Dα1 or Dβ2 nicotinic acetylcholine receptor subunits can confer resistance to neonicotinoids in Drosophila melanogaster. *Insect Biochem. Mol. Biol.* (2008). doi:10.1016/j.ibmb.2007.12.007

38. Xu, X. *et al.* Pharmacological characterization of cis-nitromethylene neonicotinoids in relation to imidacloprid binding sites in the brown planthopper, Nilaparvata lugens. *Insect Mol. Biol.* (2010). doi:10.1111/j.1365-2583.2009.00923.x

39. Liu, M. Y. & Casida, J. E. High affinity binding of [3h]imidacloprid in the insect acetylcholine receptor. *Pestic. Biochem. Physiol.* (1993). doi:10.1006/pest.1993.1034

40. Cheng, H. *et al.* Crystallization scale purification of α7 nicotinic acetylcholine receptor from mammalian cells using a BacMam expression system. *Acta Pharmacol. Sin.* (2015). doi:10.1038/aps.2015.34

41. Maldonado-Hernández, R., Quesada, O., Colón-Sáez, J. O. & Lasalde-Dominicci, J. A. Sequential purification and characterization of Torpedo californica nAChR-DC supplemented with CHS for high-resolution crystallization studies. *Anal. Biochem.* (2020). doi:10.1016/j.ab.2020.113887

42. Wut, P. *et al.* The Drosophila acetylcholine receptor subunit Dα5 is part of an α-bungarotoxin binding acetylcholine receptor. *J. Biol. Chem.* (2005). doi:10.1074/jbc.M409639200

43. Quesada, O. *et al.* Uncovering the lipidic basis for the preparation of functional nicotinic acetylcholine receptor detergent complexes for structural studies. *Sci. Rep.* (2016). doi:10.1038/srep32766

44. Barnstedt, O. *et al.* Memory-Relevant Mushroom Body Output Synapses Are Cholinergic. *Neuron* (2016). doi:10.1016/j.neuron.2016.02.015

45. Perry, T., Somers, J., Yang, Y. T. & Batterham, P. Expression of insect α6-like nicotinic acetylcholine receptors in Drosophila melanogaster highlights a high level of conservation of the receptor: Spinosyn interaction. *Insect Biochem. Mol. Biol.* (2015). doi:10.1016/j.ibmb.2015.01.017

46. Kondo, S. *et al.* Neurochemical Organization of the Drosophila Brain Visualized by Endogenously Tagged Neurotransmitter Receptors. *Cell Rep.* (2020). doi:10.1016/j.celrep.2019.12.018

47. Korona, D. *et al.* Characterisation of protein isoforms encoded by the drosophila glycogen synthase kinase 3 gene shaggy. *PLoS One* (2020). doi:10.1371/journal.pone.0236679

48. Korona, D., Koestler, S. & Russell, S. Engineering the Drosophila Genome for Developmental Biology. *J. Dev. Biol.* **5**, 16 (2017).

49. Geladaki, A. *et al.* Combining LOPIT with differential ultracentrifugation for high-resolution spatial proteomics. *Nat. Commun. 2019 101* **10**, 331 (2019).

50. Shevchenko, A., Tomas, H., Havliš, J., Olsen, J. V. & Mann, M. In-gel digestion for mass spectrometric characterization of proteins and proteomes. *Nat. Protoc.* (2007). doi:10.1038/nprot.2006.468

51. Queiroz, R. M. L. *et al.* Comprehensive quantitation of RNA-protein interaction

dynamics by orthogonal organic phase separation (OOPS) Europe PMC Funders Group. *Nat Biotechnol* (2019).

52. Rappsilber, J., Mann, M. & Ishihama, Y. Protocol for micro-purification, enrichment, pre-fractionation and storage of peptides for proteomics using StageTips. *Nat. Protoc.* (2007). doi:10.1038/nprot.2007.261

53. Gobom, J., Nordhoff, E., Mirgorodskaya, E., Ekman, R. & Roepstorff, P. Sample purification and preparation technique based on nano-scale reversed-phase columns for the sensitive analysis of complex peptide mixtures by matrix-assisted laser desorption/ionization mass spectrometry. *J. Mass Spectrom.* (1999). doi:10.1002/(SICI)1096-9888(199902)34:2<105::AID-JMS768>3.0.CO;2-4

54. Koenig, T. *et al.* Robust prediction of the MASCOT score for an improved quality assessment in mass spectrometric proteomics. *J. Proteome Res.* (2008). doi:10.1021/pr700859x

55. Eng, J. K., McCormack, A. L. & Yates, J. R. An approach to correlate tandem mass spectral data of peptides with amino acid sequences in a protein database. *J. Am. Soc. Mass Spectrom.* (1994). doi:10.1016/1044-0305(94)80016-2

56. Ihaka, R. & Gentleman, R. R: A Language for Data Analysis and Graphics. *J. Comput. Graph. Stat.* (1996). doi:10.1080/10618600.1996.10474713

57. Rstudio, T. RStudio: Integrated Development for R. *Rstudio Team, PBC, Boston, MA URL http://www.rstudio.com/* (2020). doi:10.1145/3132847.3132886

58. Ginestet, C. ggplot2: Elegant Graphics for Data Analysis. *J. R. Stat. Soc. Ser. A (Statistics Soc.* (2011). doi:10.1111/j.1467-985x.2010.00676_9.x

59. Krogh, A., Larsson, B., Von Heijne, G. & Sonnhammer, E. L. L. Predicting transmembrane protein topology with a hidden Markov model: Application to complete genomes. *J. Mol. Biol.* (2001). doi:10.1006/jmbi.2000.4315

60. Tsirigos, K. D., Elofsson, A. & Bagos, P. G. PRED-TMBB2: Improved topology prediction and detection of beta-barrel outer membrane proteins. in *Bioinformatics* (2016). doi:10.1093/bioinformatics/btw444

61. Blanc, M. *et al.* SwissPalm: Protein Palmitoylation database. *F1000Research* (2015). doi:10.12688/f1000research.6464.1

62. Pierleoni, A., Martelli, P. & Casadio, R. PredGPI: A GPI-anchor predictor. *BMC Bioinformatics* (2008). doi:10.1186/1471-2105-9-392

63. Bologna, G., Yvon, C., Duvaud, S. & Veuthey, A. L. N-terminal myristoylation predictions by ensembles of neural networks. *Proteomics* (2004). doi:10.1002/pmic.200300783

64. Carbon, S. *et al.* The Gene Ontology Resource: 20 years and still GOing strong. *Nucleic Acids Res.* (2019). doi:10.1093/nar/gky1055

65. Huang, D. W., Sherman, B. T. & Lempicki, R. A. Systematic and integrative analysis of large gene lists using DAVID bioinformatics resources. *Nat. Protoc.* (2009). doi:10.1038/nprot.2008.211

66. Goddard, T. D. *et al.* UCSF ChimeraX: Meeting modern challenges in visualization and analysis. *Protein Sci.* (2018). doi:10.1002/pro.3235

67. Mitchell, A. L. *et al.* InterPro in 2019: Improving coverage, classification and access to protein sequence annotations. *Nucleic Acids Res.* (2019). doi:10.1093/nar/gky1100

68. Liu, W. *et al.* IBS: An illustrator for the presentation and visualization of biological sequences. *Bioinformatics* (2015). doi:10.1093/bioinformatics/btv362

69. Madeira, F. *et al.* The EMBL-EBI search and sequence analysis tools APIs in 2019. *Nucleic Acids Res.* (2019). doi:10.1093/nar/gkz268

Acknowledgements

We thank Professor Dr. Tim Dafforn for kindly providing us styrene maleic acid (SMA) copolymer, Joao A. Paulo, Ph.D. for helpful exchange and Mrs Renata Feret for technical discussions. Funding was provided by BBSRC (BB/P021107/1) and Syngenta. We are very grateful to Syngenta and the Milner Therapeutics Institute for great infrastructural support. Electron microscopy was performed using the facilities at CAIC.

Author Contributions

Overall design and conception were performed by B.D., D.K., C.N.G.G., L.C., F.E., S.R., and K.S.L.. Experimental data were achieved by D.K., B.D., C.N.G.G., R.M.L.Q., G.J., M.J.D., D.P.M. and K.H.M.. Data examination was performed by B.D., C.N.G.G., R.M.L.Q., D.P.M., and D.K.. Manuscript preparation was conducted by B.D., D.K., C.N.G.G., L.C.F., F.E., S.R., and K.S.L. with contributions of all authors.

Additional information

Proteomics raw data will be provided after publishing in a peer-review journal.

Supplementary information

Biochemical source data and supplementary tables will be provided after publishing in a peer-review journal.

Conflict of interest

The authors declare no conflict of interests.

Figures

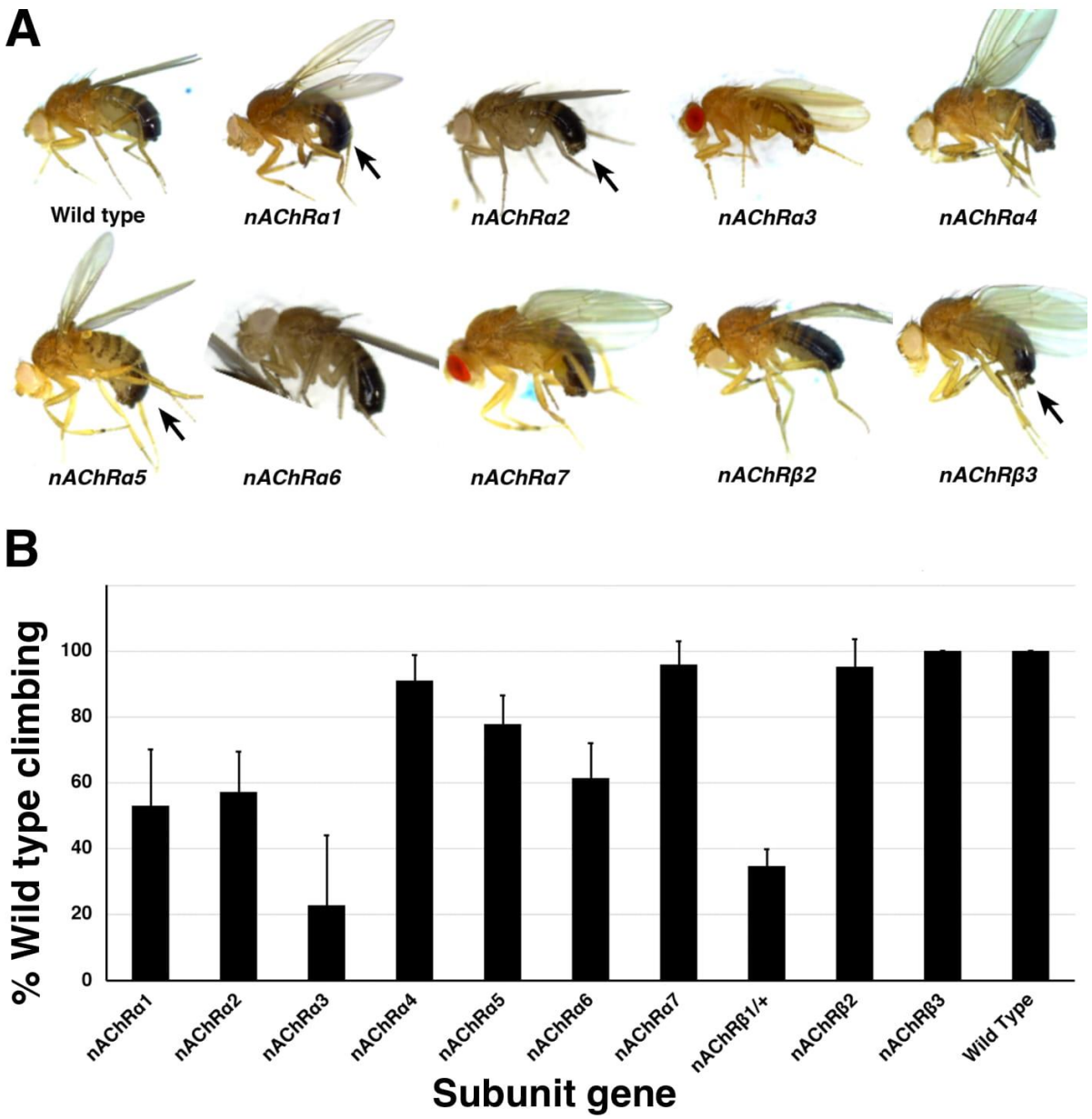

Fig 1. Morphological and locomotor phenotypes in *nAChR* subunit mutants.
A. Adult males from indicated *nAChR* subunit null mutants. Arrows indicate strong curled abdomen phenotypes. **B** Graph of locomotor activity determined in climbing assays as a percentage of wild type. Error bars represent standard deviation from 5 replicates.

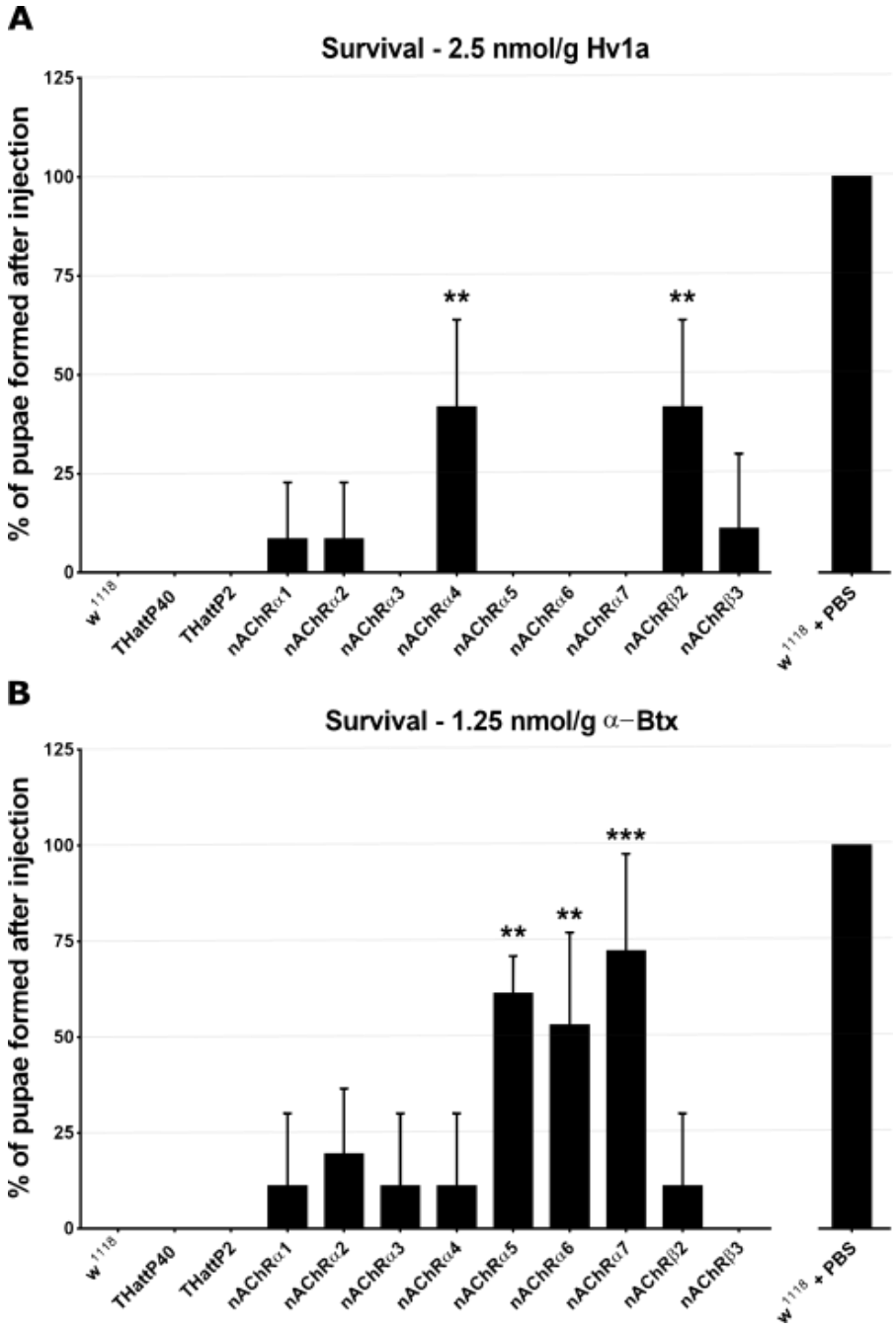

Fig 2. ω-Hexatoxin-Hv1a and α-Bungarotoxin target different nAChR subunits.
A. Bar graph of the survival rate, measured as the percentage of pupae formed, following larval injection of 2.5 nmol/g Hv1a in the indicated homozygous lines. Mean ± SD of 3 independent replicates of 10 larvae per replicate. ***P*=0.0035 (one-way ANOVA ($F_{(11,24)}$=4.99, *P*=0.0005 with Bonferroni's multiple comparisons test). 3 independent replicates in each group (10 injected larvae in total). **B.** Survival rate following larval injection of 1.25 nmol/g α-Btx. Mean ± SD of 3 independent replicates of 10 larvae per replicate. ***P*<0.001, ****P*=0.0001 (one-way ANOVA ($F_{(11,24)}$= 7.921, *P*<0.0001, followed by Bonferroni's multiple comparisons test). 3 independent replicates in each group (10 injected larvae in total). w^{1118} is the wild type base stock, *THattp40* and *THattP2* are the Cas9 lines used to establish the mutants, w^{1118} + PBS represents the injection control.

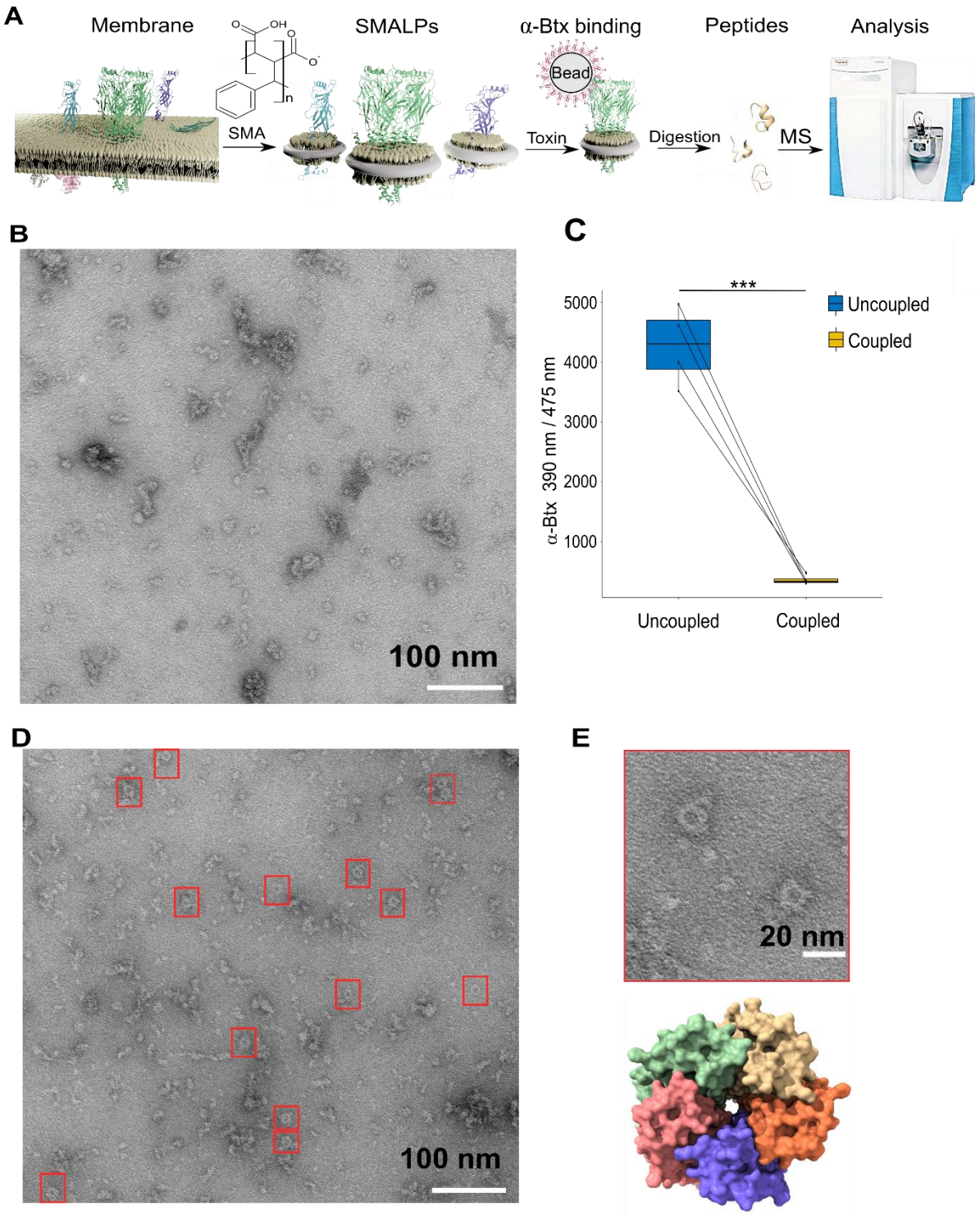

Fig 3. Forming styrene maleic acid lipid particles (SMALPs)

A. Schematic representation of the SMALPs extraction and nAChRs pull-down for mass spectrometric analysis. **B.** Negative staining of extracted SMALPs by transmission electron microscopy. Scale bar 100 nm. **C.** Fluorescence signal of uncoupled α-Btx in solution before and after coupling to affinity beads (two-tailed t-test, ***P<0.001, n=4). **D and E.** Negative staining of extracted SMALPs after α-Btx pull-downs. Ring-like protein structures are boxed (Scale bar = 100 nm) with an example in the magnified image (Scale bar = 20 nm). A top view of the nAChR structure from PDB entry 4HQP is shown for reference.

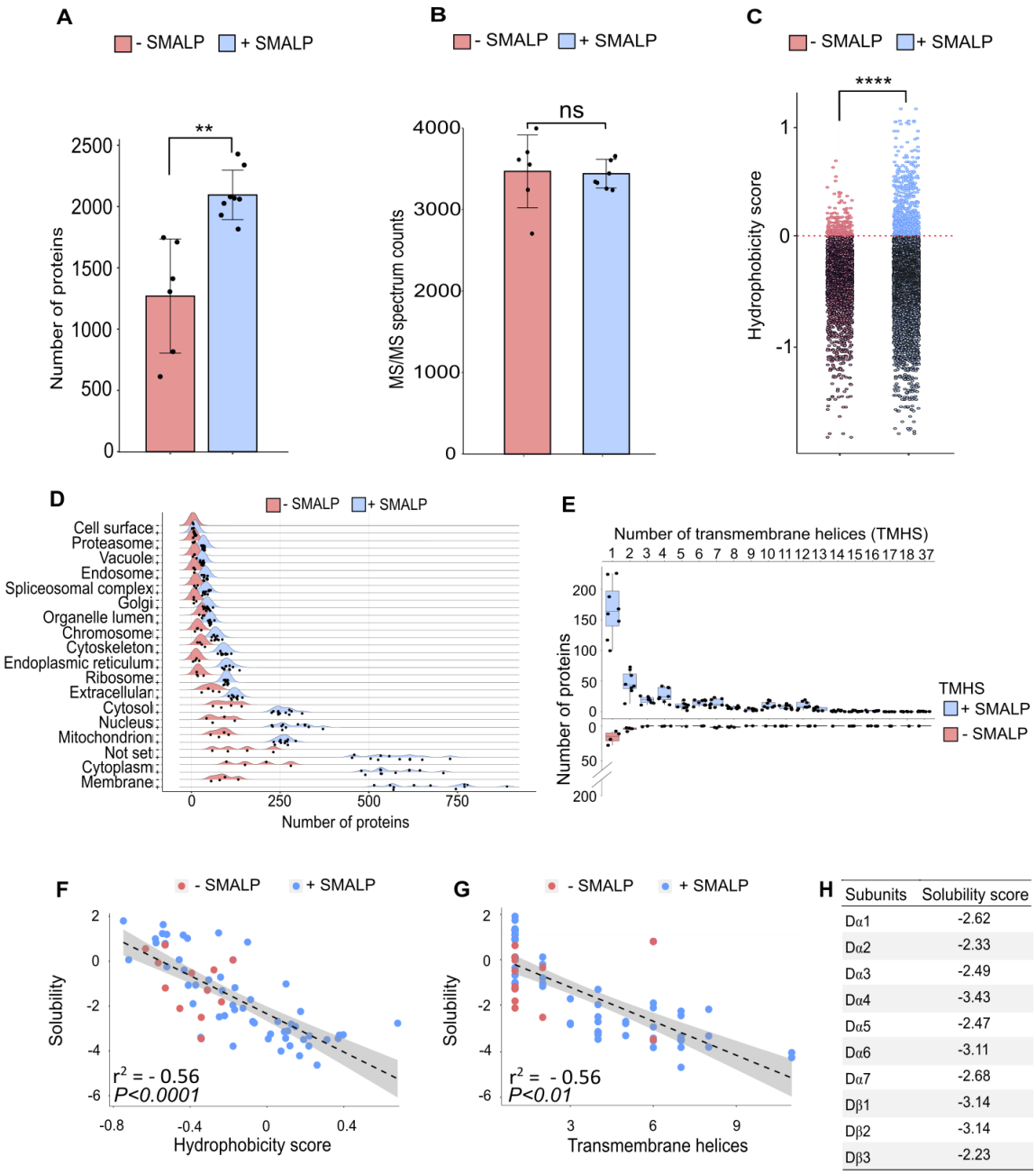

Fig 4. Identification of proteins enriched by SMALP extraction

A. Number of identified proteins in affinity pull-down samples solubilized with or without SMA, two-tailed t-test, ***P*<0.01, n=6 or 8 replicates per condition. **B.** MS/MS spectrum counts from samples solubilized with or without SMA, ns = not significant after two-tailed t-test with n=6 or 8. **C.** Calculated hydrophobicity score of amino acid residues found in protein sequences obtained with and without SMA solubilisation, *****P*<0.0001, two-tailed t-test, n=3 per condition. **D.** GO term (cellular compartment) enrichment of proteins identified with and without SMA solubilisation, n=4 or 11. **E.** Predicted numbers of proteins containing transmembrane helices obtained with or without SMA solubilisation, n=4 or 8. **F and G.** Analysis of solubility and hydrophobicity of receptors identified with and without SMA solubilisation (r^2= -0.56, *P*<0.0001, n=4) and of transmembrane receptor helices (r^2=0.56, *P*<0.01, n=4). **H.** Solubility score of individual nAChR subunits.

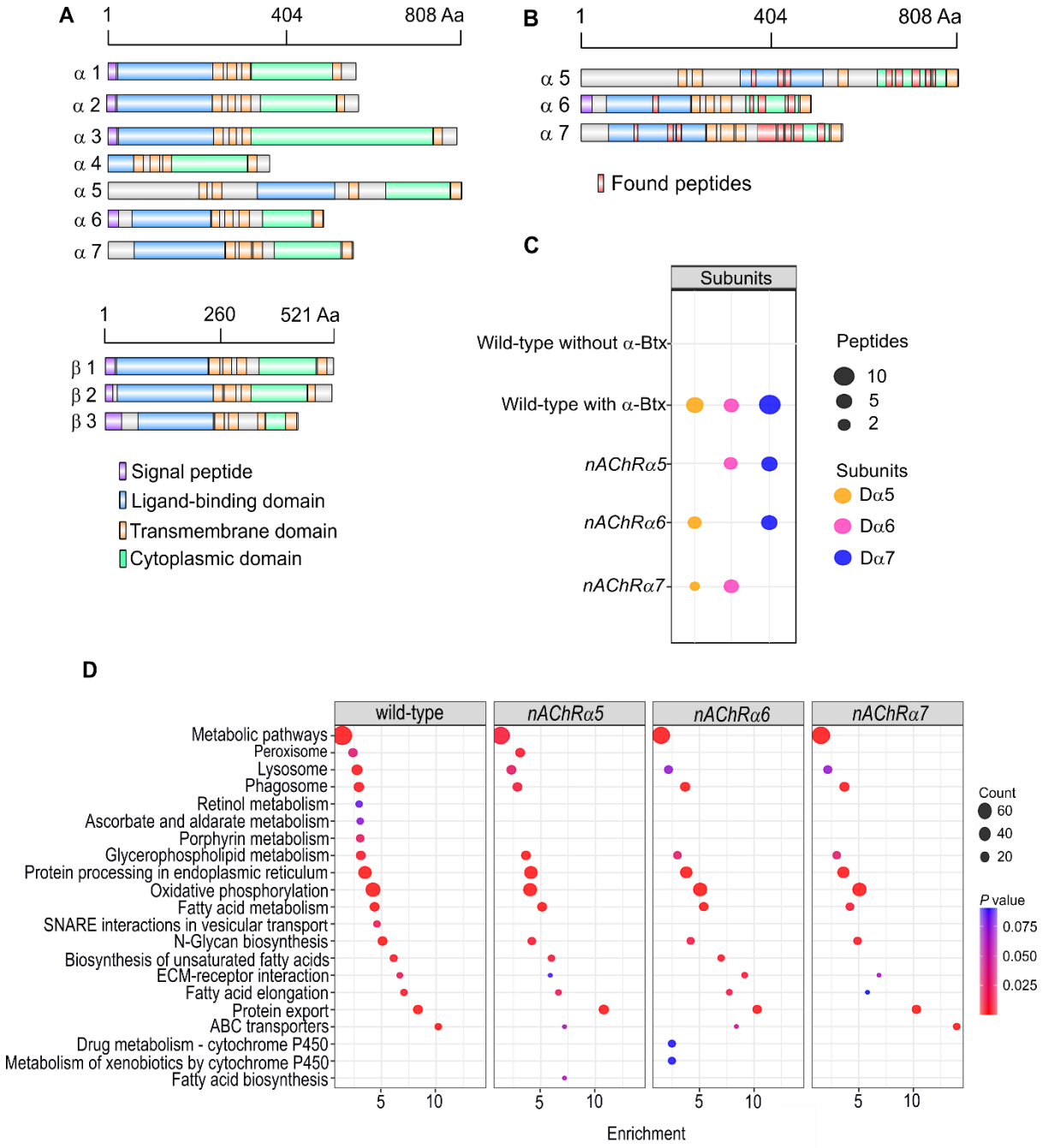

Fig 5 Three nAChR α-subunits are binding to α-bungarotoxin (α-Btx)

A Graphical representation of ten nAChR subunits. The position of protein domains and signal peptides are shown. **B** Identified peptides of Dα5, Dα6 and Dα7 nAChR subunits in pull-downs using α-Btx affinity beads. Found peptides in ligand-binding and cytoplasmic domain are highlighted in red. **C** Numbers of identified unique peptides in wild-type pull-downs using affinity beads in absence and presence of α-Btx, n=3. Deleting *nAChRα5, nAChRα6, nAChRα7* and performing pull-downs identified unique peptides of nAChR subunits suggesting that functional complexes can be formed in null alleles, n=3. **D** KEGG pathway enrichment analysis of pull-downs in wild-type and *nAChRα5, nAChRα6, nAChRα7* null alleles, Fisher's exact test, n=3. Protein counts with *P* values of enriched pathways are shown. *P* values of ≤ 0.05 are to be considered as strongly enriched with default threshold of 0.1.

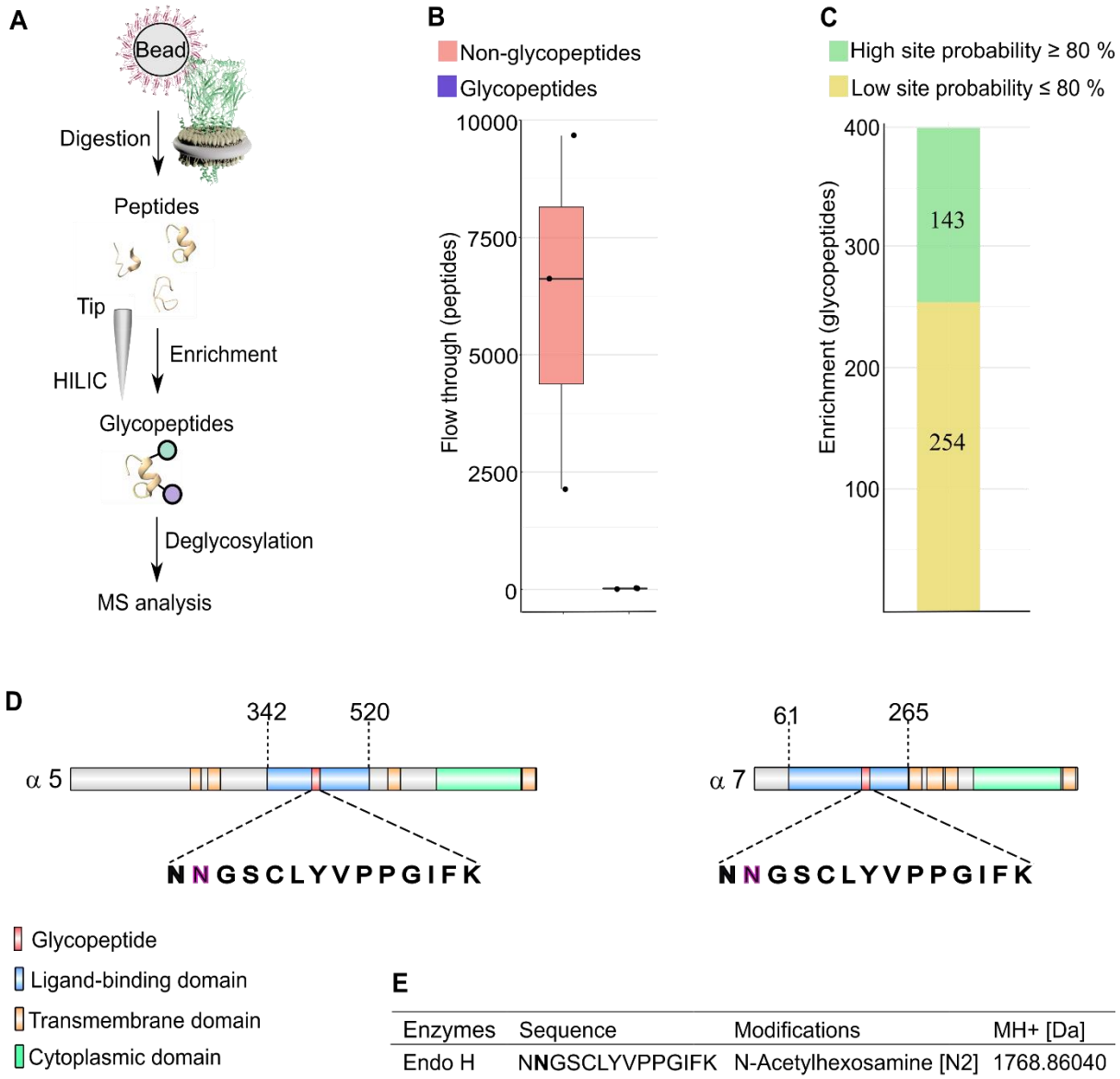

E

Enzymes	Sequence	Modifications	MH+ [Da]
Endo H	NNGSCLYVPPGIFK	N-Acetylhexosamine [N2]	1768.86040
PNGase F	NNGSCLYVPPGIFK	Deamidated [N2]	1566.75456

Fig 6. N-glycosylation sites in nAChR subunits

A. Diagrammatic representation of nAChR subunit glycopeptide enrichment. Pull-downs with α-Btx affinity beads enrich for nAChRs and after tryptic digestion glycopeptides were enriched. Glycopeptides were deglycosylated with Endo H or PNGase F and analyzed my mass spectrometry. **B.** Low numbers of glycopeptides (average 20) are detected in flow through fractions. **C.** Numbers of identified glycopeptides according to site probabilities are shown (n=3). **D.** Shared glycopeptide identified in the ligand-binding domain of Dα5 and Dα7, an N-linked glycosylated asparagine (N) residue is highlighted. **E.** Deglycosylated peptide with either Endo H or PNGase F and contains either an N-acetylhexosamine or is deamidated on asparagine (N2). The two different modifications on the same peptide lead to a different monoisotopic mass (MH+ [Da]). Peptide contains an additional carbamidomethyl on cysteine (C5).

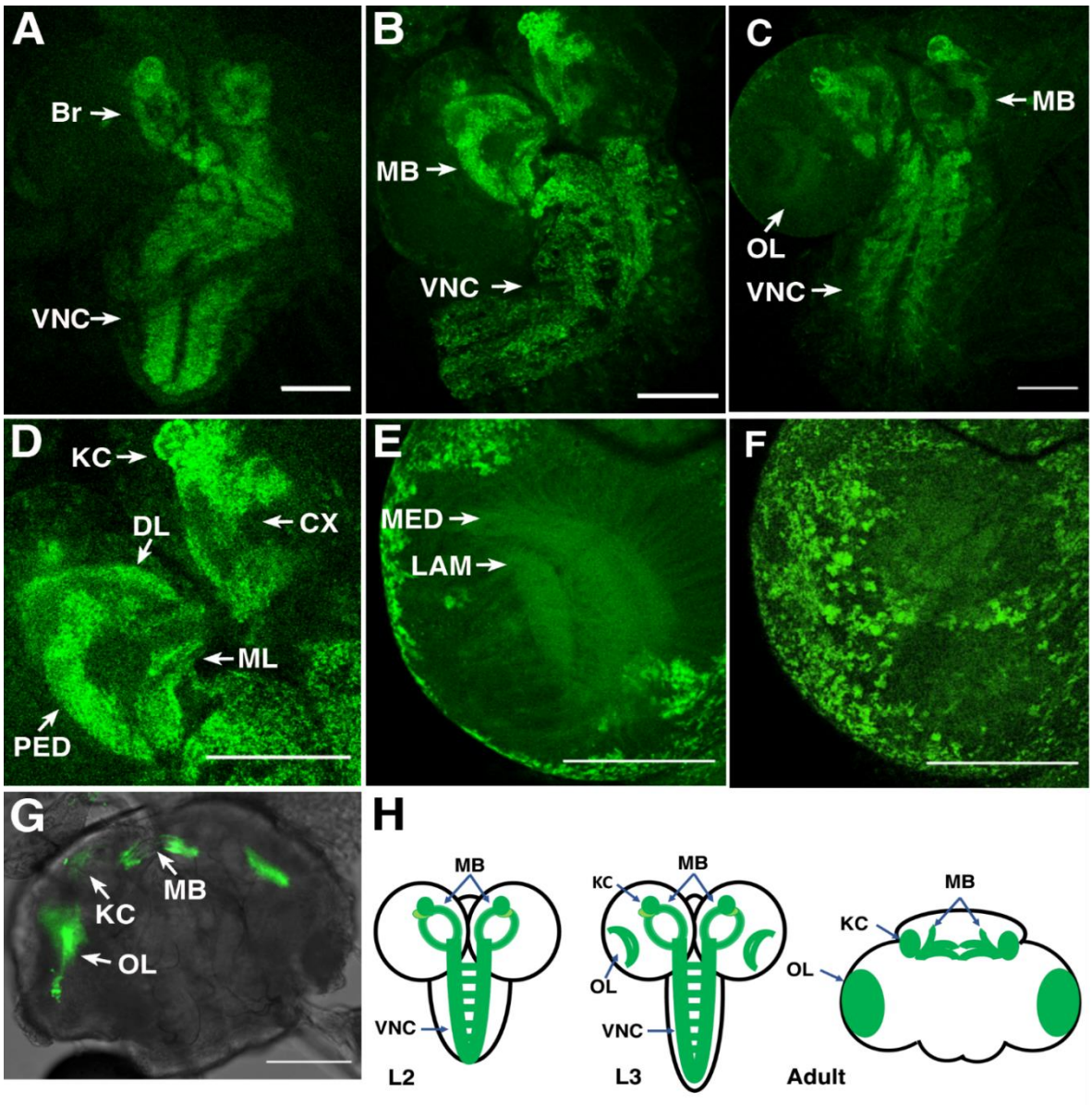

Fig 7. *In vivo* imaging of endogenously tagged Dα6 nAChR subunit

A-G. Live imaging of fly brains carrying a C-terminal EGFP fusion into the endogenous *nAChRα6* locus. **A-C.** Dα6 subunit in 2nd, early and late 3rd instar larvae brain, respectively. Visible localization in ventral nerve cord (VNC), mushroom bodies (MB), and optic lobes (OL). Scale bar = 100 μm**. D.** Dα6 subunit in mushroom bodies of 3rd instar larvae with detectable fluorescence signal in Kenyon cells (KC), calyx (CX), peduncle (PED), dorsal lobes (DL) and medial lobes (ML). Scale bar = 100 μm**. E.** Dα6 subunit was observed in developing optic lobes, lamina (LAM) and medulla (MED) of later 3rd instar larvae. Scale bar = 100 μm. **F.** Dα6 subunit on the external structures of developing lobes in later 3rd instar larvae. Scale bar = 100 μm. **G.** Dα6 subunit in adult fly brain, strong signal detected in mushroom bodies (MB) and optic lobe (OL). Scale bar = 100 μm**. H.** Schematic summary of Dα6 subunit expression during different developmental stages, 2nd and 3rd instar larvae and adult fly, (L2, L3 and Adult, respectively) in which the green lines indicate the localization of the Dα6 subunit.

Supplementary Figures

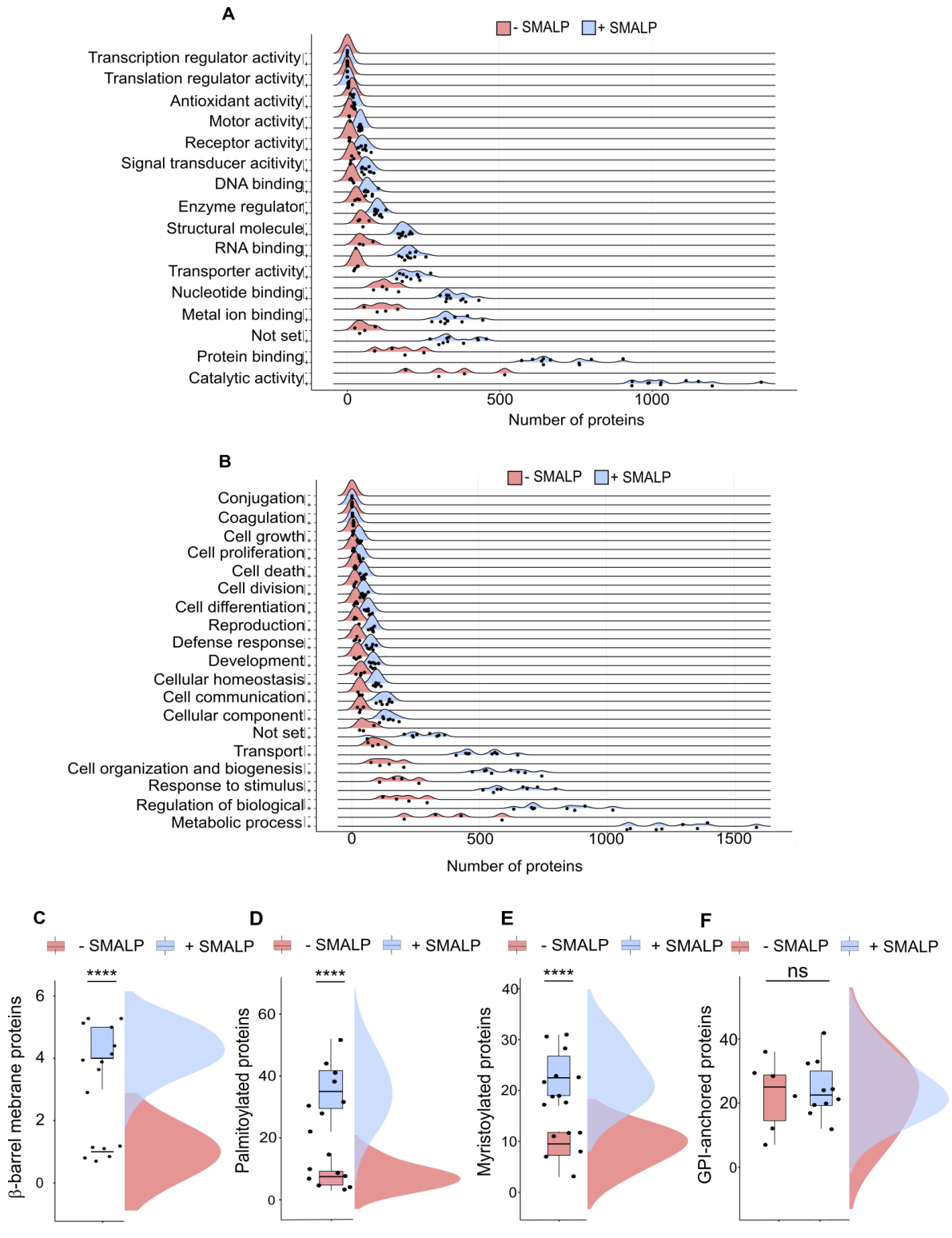

Fig. S1 GO terms and predicted membrane proteins

A GO slim term for biological process and (**B**) for molecular function analysed within samples solubilized without or with SMA, n=4 or 11 per conditions. Predicted β-barrel membrane- (**C**), two-tailed t-test ****P<0.0001, n=6 or 10; palmitoylated- (**D**), ****P<0.0001, each n=8; myristoylated- (**E**), ****P<0.0001, n=6 or 10; and GPI-anchored proteins (**F**), non-significant ns, n=6 or 10.

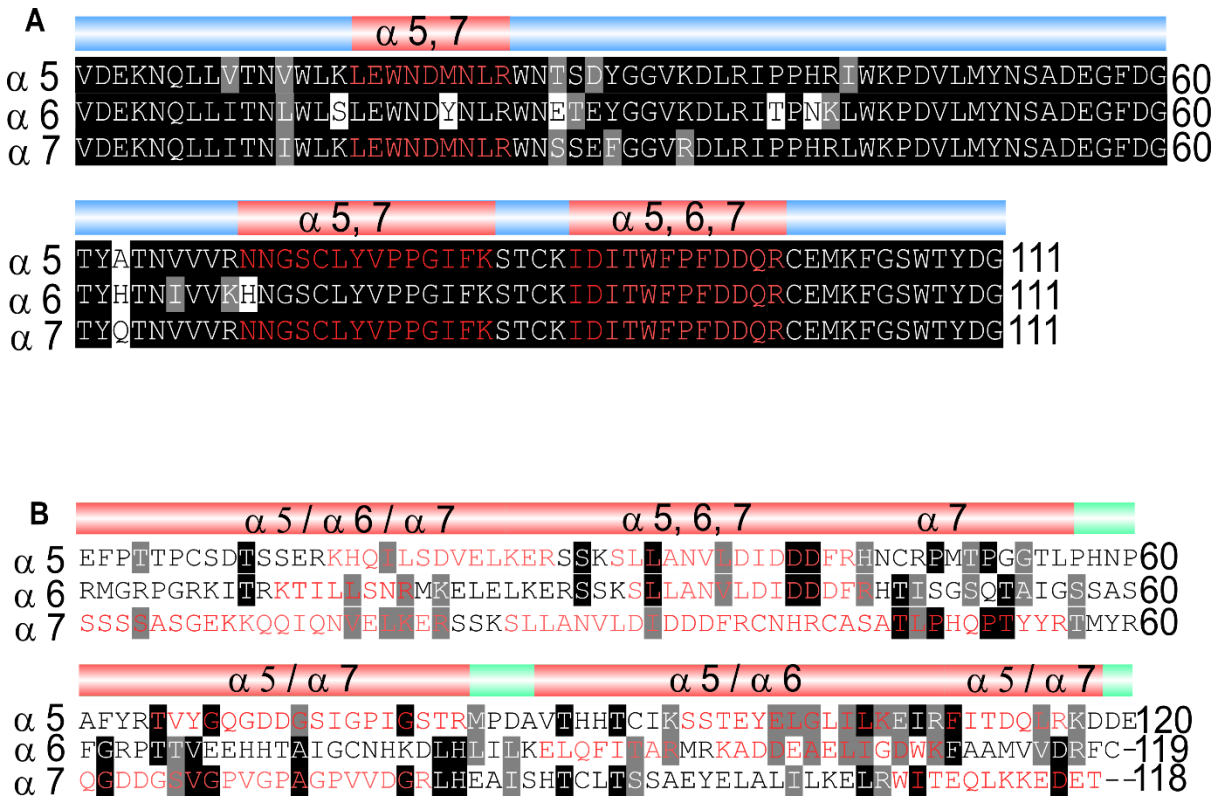

Fig. S2 Identified peptides in ligand-binding and cytoplasmic domain

A Shared peptides found in the ligand-binding domains are shown in red. **B** Identified unique (/) and shared (,) peptides in cytoplasmic domains.

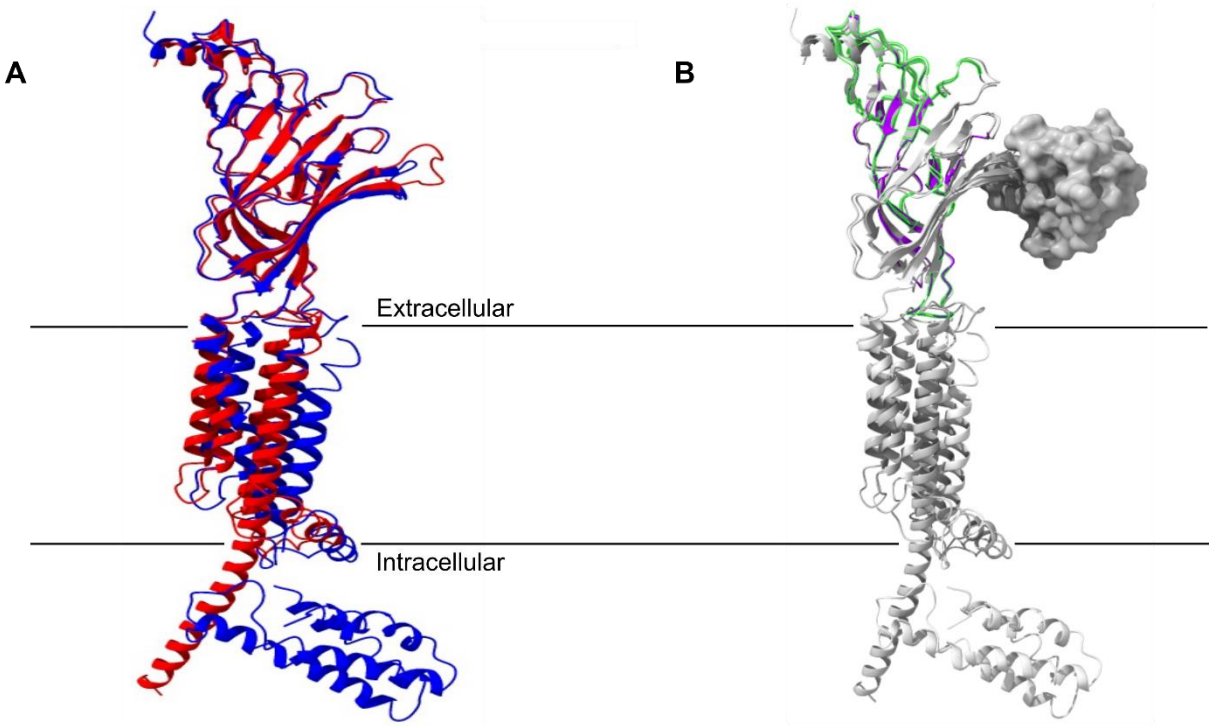

Fig. S3 Superimposed nAChR α-subunits structure together with identified peptides
A Superimposed nAChR α-subunit structures from *Homo sapiens* (blue, PDB 6USF) and *Torpedo californica* (red, 6UWZ). Extracellular ligand-binding domain (LBD) illustrates a structure similarity. **B** Same superimposed structures bound to α-bungarotoxin (α-Btx, surface structure). Peptides found in LBD are highlighted in green. The homology regions of Dα6 nAChRs LBD are shown in violet.

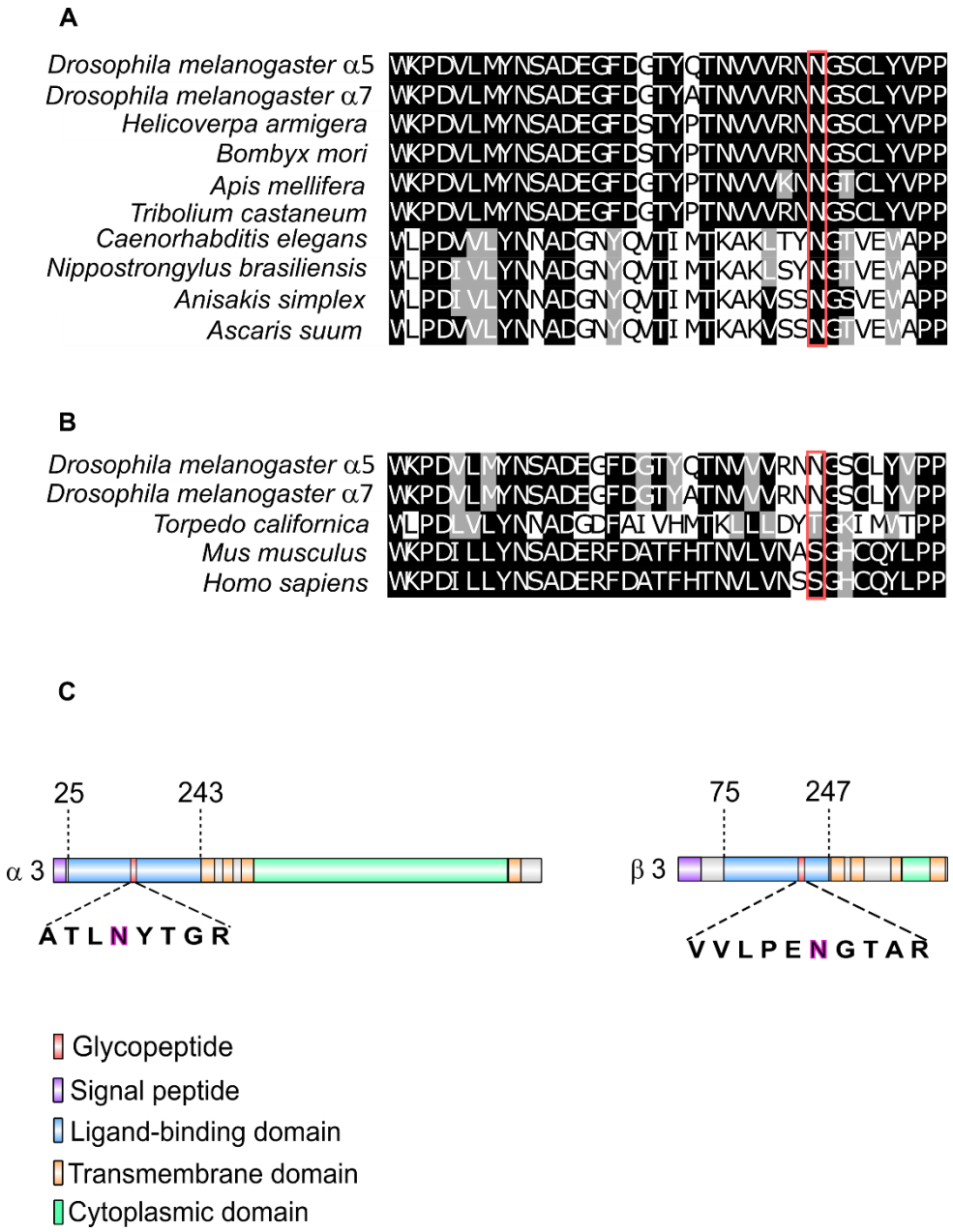

Fig. S4 Glycosylation sites of nAChR subunits

A Multiple sequence alignment of insect α7 nAChR subunits compared to sequences of nematodes. The glycosylated ligand-binding domain (LBD) sequence of Dα5 and Dα7 nAChR subunits are shown. Glycosylated asparagine residues highlighted in red are conserved within insects and nematodes (Dα5 422 and Dα7 170 amino acids). **B** Same Dα5 and Dα7 nAChR subunit sequences compared to *T.californica*, *D.rerio*, *M. musculus* and *H. sapiens*. **C** Graphical representation of Dα3 and Dβ3 nAChR subunits. N-acetylhexosamine (H) modification on asparagine residues are highlighted and are of low site probability ≤ 80 %.